ELECTROMAGNETIC MODELING OF HIGH-SPEED INTERCONNECTS WITH FREQUENCY DEPENDENT CONDUCTOR LOSSES, COMPATIBLE WITH PASSIVE MODEL ORDER REDUCTION TECHNIQUES

by

Soheila Pasha

A Dissertation Submitted to the Faculty of the

DEPARTMENT OF ELECTRICAL AND COMPUTER ENGINEERING

In Partial Fulfillment of the Requirements
For the Degree of

DOCTOR OF PHILOSOPHY

In the Graduate College

THE UNIVERSITY OF ARIZONA

2012

THE UNIVERSITY OF ARIZONA
GRADUATE COLLEGE

As members of the Dissertation Committee, we certify that we have read the dissertation prepared by Soheila Pasha
entitled Electromagnetic Modeling of High-Speed Interconnects with Frequency Dependent Conductor Losses, Compatible with Passive Model Order Reduction Techniques and recommend that it be accepted as fulfilling the dissertation requirement for the Degree of Doctor of Philosophy

_____Date: 11/20/2012
Steven L. Dvorak, Ph.D.

_____Date: 11/20/2012
Kathleen L. Melde, Ph.D.

_____Date: 11/20/2012
Janet Meiling Roveda, Ph.D.

Final approval and acceptance of this dissertation is contingent upon the candidate's submission of the final copies of the dissertation to the Graduate College.
I hereby certify that I have read this dissertation prepared under my direction and recommend that it be accepted as fulfilling the dissertation requirement.

_____Date: 11/20/2012
Dissertation Director: Steven L. Dvorak, Ph.D.

STATEMENT BY AUTHOR

This dissertation has been submitted in partial fulfillment of requirements for an advanced degree at The University of Arizona and is deposited in the University Library to be made available to borrowers under rules of the Library.

Brief quotations from this thesis are allowable without special permission, provided that accurate acknowledgment of source is made. Requests for permission for extended quotation from or reproduction of this manuscript in whole or in part may be granted by the head of the major department or the Dean of the Graduate College when in his or her judgment the proposed use of the material is in the interests of scholarship. In all other instances, however, permission must be obtained from the author.

SIGNED: _____

ACKNOWLEDGMENTS

I would like to express my sincere gratitude to my advisor Dr. Dvorak for his guidance, support, technical insights, and invaluable inputs. I would like to thank Dr. Melde for her continued support and encouragement, and editorial feedback. I am appreciative of my committee members, Dr. Dvorak, Dr. Melde and Dr. Wang for their efforts and constructive comments.

I am indebted to Dr. Cangellaris for his constant guidance and immense technical support throughout this project. I would like to extend my acknowledgment to late Dr. Prince who provided support and gave me the opportunity to work on this exciting research. The financial support from SRC is greatly appreciated. I am also grateful to Dr. Celik for his technical support. I would like to appreciate the administrative support of Tami Whelan during these years.

Last but not least, I would like to thank my family for their support and dedication.

To:

My husband, Amirmasoud

and

My daughter, Sahar

TABLE OF CONTENTS

LIST OF FIGURES 8
ABSTRACT 10
CHAPTER 1 INTRODUCTION 11
CHAPTER 2 EQUIVALENT SKIN-EFFECT MODELS 14
2.1 Introduction 14
2.2 Development of the Magnetic Vector Potential Integral Equation 14
2.3 Development of the Current Density Integral Equation 17
2.4 Method of Moments 25
2.5 Inductance and Resistance Matrices 29
CHAPTER 3 NEW EFFICIENT AND PASSIVE MULTI-CONDUCTOR TRANSMISSION LINE MODEL 33
3.1 Introduction 33
3.2 The Semi-Discrete Interconnect Model 34
3.3 The Use of Compact Differences 41
3.4 Passivity of the Discrete Transmission Line 48
3.5 Discrete Model of an MTL 52
CHAPTER 4 NEW EFFICIENT AND PASSIVE FREQUENCY DEPENDENT MULTI-CONDUCTOR TRANSMISSION LINE MODEL 57
4.1 Introduction 57
4.2 Discrete Model of Interconnects with Frequency Dependent Self Ohmic Loss 59
4.2.1 Approximation of the Diagonal Elements of $\hat{Z}(s)$ 68
4.2.2 Approximation of Off-Diagonal Elements of $\hat{Z}(s)$ 70
4.2.3 Positive-Definiteness of $\hat{Z}(s)$ 71
4.2.4 Summary of the Overall Algorithm 73
4.3 Discrete Model of Interconnects with Frequency Dependent Self and Mutual Ohmic Loss 74
4.3.1 Development of the Discrete Model 77
CHAPTER 5 MODEL ORDER REDUCTION TECHNIQUES 81

TABLE OF CONTENTS, Continued

5.1 Asymptotic Waveform Evaluation (AWE) 83
5.2 Passive Reduced-Order Interconnect Macromodeling Algorithm (PRIMA) 86
CHAPTER 6 NUMERICAL ANALYSIS 90
6.1 Efficient Passive Interconnect Model (UA-EPIM) for a Single TL 90
6.2 Efficient Passive Interconnect Model (UA-EPIM) for MTL 95
6.3 Dispersive Efficient Passive Interconnect Model (UA-DEPIM1) for the Case of Frequency Dependent Self Ohmic Loss 100
6.4 Dispersive Efficient Passive Interconnect Model (UA-DEPIM2) for the Case of Frequency Dependent Self and Mutual Ohmic Loss 106
CHAPTER 7 CONCLUSION 110
REFERENCES 114

LIST OF FIGURES

Figure 2.1 The point of observation with respect to the current source.....20
Figure 2.2 The method of images is used to include a reference ground plane into the system of transmission lines. 22
Figure 4.1 Modal network representation of a losssy conductor 61
Figure 4.2 Discritization of conductor cross sections in an MTL for the purpose of frequency-dependent current distribution calculation. 65
Figure 5.1 Processing of a linear sub-system into M port macromodel represented by its Y parameter matrix. 82
Figure 6.1 The circuit inside the dashed-line is represented by a 2-port Y-parameter marcromodel. Interconnects are modeled using fourth-order compact difference operators. 91
Figure 6.2 Comparison of the simulated output voltage waveform V_{out} for the interconnect circuit in Figure 6.1. 92
Figure 6.3 The magnitude of the frequency response of Y_{11} for the interconnect circuit in Figure 6.1. 93
Figure 6.4 The phase of the frequency response of Y_{11} for the interconnect circuit in Figure 6.1. 94
Figure 6.5 A circuit representing an on-chip interconnect system. The circuit inside the dashed line is represented by a 4-port Y-parameter macromodel. 96
Figure 6.6 The magnitude of the frequency response of Y_{11} for the circuit of Figure 6.5. 98
Figure 6.7 The simulated output voltage waveforms for the interconnection circuit in Figure 6.5. 99
Figure 6.8 Comparison of the Padé approximation for the real part of the p.u.l. impedance z_{11} with the calculated value, obtained numerically from (4.16). 101
Figure 6.9 Comparison of the Padé approximation for the imaginary part of the p.u.l. impedance z_{11} with the calculated value, obtained numerically from (4.16). 102

Figure 6.10 Magnitude of Y_{11} for the multiport interconnect of Figure 6.5. 103

Figure 6.11 Calculated waveform at the output of the active line of the interconnect circuit in Figure 6.5. Solid line is for the case of frequency-dependent impedance while dashed line is for frequency independent impedance. 104

Figure 6.12 Calculated waveform at the output of the quiet line of the interconnect circuit in Figure 6.5. Solid line is for the case of frequency-dependent impedance while dashed line is for frequency independent impedance. 105

Figure 6.13 The high-speed digital interconnect circuit used in the simulations. 106

Figure 6.14 Comparison between the Padé approximation of the real part of the p.u.l. impedance z_{11} and the exact value. 107

Figure 6.15 Comparison between the Padé approximation of imaginary.....108

Figure 6.16 Waveform at the output of the active line of the circuit in Figure 6.13. 109

ABSTRACT

A computationally efficient, discrete model is presented for transmission line analysis and passive model order reduction of high-speed interconnect systems. The development of this model was motivated by the on-going efforts in chip/package co-design to route a major portion of the on-chip clock and high-speed data buses through the package in order to overcome the bandwidth reduction and delay caused by the high ohmic loss of on-chip wiring. The geometric complexity of the resulting interconnections is such that model order reduction is essential for rapid and accurate signal integrity assessment to support pre-layout design iteration and optimization. The modal network theory of the skin effect in conjunction with the theory of compact differences is used for the development of discrete models for dispersive, multi-conductor interconnects compatible with passive model order reduction algorithms. The passive reduced-order interconnect modeling algorithm, PRIMA, is then used on the resulting discrete model to generate a low-order, multi-port macromodel for interconnect networks. Numerical examples are used to demonstrate the validity and efficiency of the proposed model.

CHAPTER 1 INTRODUCTION

As the trend continues toward faster, larger, and more complex integrated circuits, interconnect skin effect becomes an important factor in signal integrity studies. Moreover, the wiring pitch is rapidly shrinking, enhancing coupling and proximity effects. In such structures, signals with short rise/fall time are drastically distorted due to dispersion associated with the frequency-dependent field penetration inside the wires. Therefore, prediction of attenuation and signal distortion in high-speed interconnects requires careful modeling of the frequency-dependent ohmic loss. Furthermore, such modeling must be affected in a way that compatibility with state-of-the-art, passive model order reduction techniques is ensured [1]. Model order reduction is critical for being able to tackle complex interconnect nets. For this purpose, Krylov subspace-based methods are more attractive since they are well conditioned. Of particular interest is the development of reduced-order macromodels that maintain the passivity of the original circuit.

In Chapter 2 resistance and inductance of conductors under quasi-TEM condition are calculated. These calculations are later used to develop an equivalent RL network representing the frequency dependent of the current distribution inside a lossy conductor at high frequencies.

A new, computationally efficient, discrete model compatible with passive, reduced-order macromodeling algorithm, (PRIMA) [2], is presented in Chapter 3 The

proposed model utilizes the theory of compact differences to reduce the number of degrees of freedom used in the discretization of the generalized Telegrapher's equations. In addition, this model can be applied for lossy interconnects with position-dependent parameters.

The aforementioned model is extended in Chapter 4 for dispersive multiconductor interconnects, which is compatible with passive, reduced-order macromodeling algorithms. In that model, a scalar order reduction technique is used to find poles and residues of each diagonal entry of the per-unit-length (p.u.l.) impedance matrix ($Z(s)=R(s)+s\,L(s)$, where s is the complex angular frequency). At first, the frequency dependences of the off-diagonal elements are ignored. In interconnection structures with weak coupling, such a model is sufficient and helps keep the number of unknowns in the discrete approximation small.

In the second part of Chapter 4 a methodology is presented to incorporate dispersion of both diagonal and off-diagonal entries of Z(s) in order to develop a discrete model that is compatible with the passive, reduced-order macromodeling algorithms. The development of such a model is based on the modal network theory of the skin effect in lossy conductors [3]. The modal network theory is applied in a manner that, in addition to the skin effect, the proximity effect, which tends to impact current distribution over the conductor cross section for closely-placed conductors, is taken into account. In particular, the form of the equivalent RL circuit representation resulting from the application of the modal network theory of the skin effect is used. Generally, the impedance matrix, Z(s), associated with such an RL network, is very large for efficient waveform simulation. Therefore, PRIMA should be used for the

development of a passive, reduced-order, pole/residue representation for the frequency-dependent, per-unit-length, resistance and inductance elements of the multiconductor transmission line. However, since the direct use of PRIMA in finding the reduced form of Z(s) from the standard Modified Nodal Analysis (MNA) representation of the equivalent RL circuit generates complex poles and residues, a result that is highly undesirable since it penalizes the efficiency of the SPICE implementation of a passive model, a methodology is proposed based on a modified version of the governing system of state equations. As a result, PRIMA generates purely real, negative poles and positive definite residue matrices for the impedance of the modified system.

From the modified representation of the system, and with the introduction of properly defined auxiliary variables, a passive discrete form of the generalized Telegrapher's equations for multiconductor transmission lines is derived. The form is such that the discrete model can be incorporated directly as an MNA stamp in a SPICE-based circuit simulator either for passive model order reduction or for direct nonlinear circuit simulation.

CHAPTER 2 EQUIVALENT SKIN-EFFECT MODELS

2.1 Introduction

Today's technology trend for faster and more complicated busses combined with decreasing voltage levels creates a tighter budget for noise and timing skew. Therefore there is a demand for more accurate interconnect models, particularly at high frequencies. These interconnect models should capture frequency dependent losses for this purpose, and the model should be developed in such a way to preserve the full wave nature of Maxwell's equations.

2.2 Development of the Magnetic Vector Potential Integral Equation

We start with the time harmonic form of Maxwell's equations

$$\nabla \times \vec{E}(\vec{r}) = -j\omega\mu\vec{H}(\vec{r}) \tag{2.1}$$

$$\nabla \times \vec{H}(\vec{r}) = \vec{J}(\vec{r}) + j\omega\varepsilon\vec{E}(\vec{r}) \tag{2.2}$$

$$\nabla \cdot \varepsilon\vec{E}(\vec{r}) = q(\vec{r}) \tag{2.3}$$

$$\nabla \cdot \mu\vec{H}(\vec{r}) = 0 \tag{2.4}$$

where $\vec{E}$ is the electric field intensity, $\vec{H}$ is the magnetic field intensity, $\vec{J}$ is electric current density, q is electric charge density, ε is the permittivity, μ is the permeability, and $\vec{r}$ is the position vector. Let's define the magnetic vector potential $\vec{A}$ as

$$\vec{B}(\vec{r}) = \nabla \times \vec{A}(\vec{r}) \tag{2.5}$$

where $\vec{B}$ is the magnetic flux density that is defined as $\vec{B}(\vec{r}) = \mu \vec{H}(\vec{r})$. Therefore (2.1) can be rewritten as

$$\nabla \times \vec{E}(\vec{r}) = -j\omega \nabla \times \vec{A}(\vec{r})$$

or

$$\nabla \times \left[E(\vec{r}) + j\omega \vec{A}(\vec{r}) \right] = 0 \tag{2.6}$$

Applying vector identity, $\nabla \times (-\nabla \varphi) = 0$, where φ is the scalar electric potential, to (2.6) thus yields

$$\vec{E}(\vec{r}) + j\omega \vec{A}(\vec{r}) = -\nabla \varphi(\vec{r})$$

or

$$\vec{E}(\vec{r}) = -j\omega \vec{A}(\vec{r}) - \nabla \varphi(\vec{r}) \tag{2.7}$$

In (2.7), the electric field $\vec{E}(\vec{r})$ is directly related to the magnetic vector potential $\vec{A}(\vec{r})$ and the scalar electrical potential $\varphi(\vec{r})$. Applying (2.7) to (2.2), we obtain

$$\nabla \times \overrightarrow{H}(\vec{r}) = \overrightarrow{J}(\vec{r}) + \omega^2 \varepsilon \vec{A}(\vec{r}) - j\omega\varepsilon \nabla \varphi(\vec{r}) \tag{2.8}$$

where the magnetic field intensity, $\overrightarrow{H}(\vec{r})$, in (2.8) is expressed only in terms of the electric current density $\overrightarrow{J}$, the magnetic vector potential $\vec{A}(\vec{r})$, and the scalar electrical potential $\varphi(\vec{r})$.

The goal is to solve the equations for the magnetic vector potential and the scalar electric potential. In order to do this, $\overrightarrow{H}(\vec{r})$ should be eliminated from equation (2.8). In addition, we need to obtain another equation for $\vec{A}(\vec{r})$ and $\varphi(\vec{r})$ to find their solutions. The first step is to take the curl of (2.5)

$$\nabla \times \vec{B}(\vec{r}) = \nabla \times \mu \vec{H}(\vec{r}) \tag{2.9}$$

$$\nabla \times \mu \vec{H}(\vec{r}) = \nabla \times \nabla \times \vec{A}(\vec{r}) \tag{2.10}$$

Assuming that the permeability, μ, is independent of position and using the vector identity $\nabla \times \nabla \times \vec{A}(\vec{r}) = \nabla(\nabla \cdot \vec{A}(\vec{r})) - \nabla^2 \vec{A}(\vec{r})$, we obtain

$$\mu \nabla \times \vec{H}(\vec{r}) = \nabla(\nabla \cdot \vec{A}(\vec{r})) - \nabla^2 \vec{A}(\vec{r}) \tag{2.11}$$

Substituting (2.11) into (2.8) and rearranging the terms yields

$$\nabla(\nabla \cdot \vec{A}(\vec{r})) - \nabla^2 \vec{A}(\vec{r}) = \mu \overrightarrow{J}(\vec{r}) + \omega^2 \mu\varepsilon \vec{A}(\vec{r}) - j\omega\mu\varepsilon \nabla \varphi(\vec{r}) \tag{2.12}$$

where there are two unknowns $\vec{A}(\vec{r})$ and $\varphi(\vec{r})$ and a known source $\vec{J}$. In order to find an equation for $\vec{A}(\vec{r})$, we use the Lorentz condition, $\varphi(\vec{r}) = -\frac{1}{j\omega\mu\varepsilon}\nabla\cdot\vec{A}(\vec{r})$. Substituting $\nabla\varphi(\vec{r})$ from the Lorentz equation into (2.12) yields

$$\nabla^2\vec{A}(\vec{r}) + \omega^2\mu\varepsilon\vec{A}(\vec{r}) = -\mu\vec{J}(\vec{r}) \tag{2.13}$$

The Integral form of the solution to this equation for a given current distribution in free space is well known:

$$\vec{A}(\vec{r}) = \frac{\mu}{4\pi}\int_v \frac{\vec{J}(\vec{r'})e^{-j\beta|\vec{r}-\vec{r'}|}}{|\vec{r}-\vec{r'}|}dv' \tag{2.14}$$

where β is the wave number and is defined as $\beta = \omega\sqrt{\mu\varepsilon}$, and $\vec{r}$ is the point at which the vector magnetic potential is evaluated.

2.3 **Development of the Current Density Integral Equation**

From Ohm's law, the current density vector, $\vec{J}$, is expressed as:

$$\vec{J} = \sigma\vec{E} \tag{2.15}$$

By substituting $\vec{E}$ from (2.7) into(2.15), the current density vector, $\vec{J}$, can be written in terms of the magnetic vector potential $\vec{A}(\vec{r})$ and the divergence of the scalar electrical potential $\varphi(\vec{r})$:

$$\vec{J} = -j\omega\sigma\vec{A} - \sigma\nabla\varphi(\vec{r}) \tag{2.16}$$

In order to calculate the current density vector, $\vec{J}$, we need to find the solution for $\nabla\varphi(\vec{r})$. Under quasi-TEM conditions, the longitudinal components of the electric and magnetic fields are negligible compared to their transverse components. Thus the magnetic vector potential, $\vec{A}(\vec{r})$, and the current density vector, $\vec{J}$, only have *z*-components, (i.e. A_z and J_z). Since $\vec{E} = \vec{J}/\sigma$ and $\vec{J}_x = \vec{J}_y = 0$, we can conclude that $E_x = \partial\varphi/\partial x = 0$ and $E_y = \partial\varphi/\partial y = 0$. Therefore, from (2.16) we see that $\nabla\varphi(\vec{r})$ only has a *z*-component as well. In future equations we will omit the subscript z for simplicity.

Let us consider a system of *M* parallel conductor transmission lines. Next we integrate both sides of equation (2.16) over the cross sectional area S_m of each conductor to calculate the total current flowing through the m^{th} conductor:

$$\iint_{S_m} J(\vec{r'})ds = -j\omega\sigma\iint_{S_m} A(\vec{r})ds - \sigma\iint_{S_m}\frac{\partial\varphi}{\partial z}ds \tag{2.17}$$

Here $\iint_{S_m} J(\vec{r'})ds$ is the total current flowing through the cross section of the m^{th} conductor. In order to calculate the second quantity on the right, we first show that $\frac{\partial\varphi}{\partial z}$ is constant over the cross sectional area of the m^{th} conductor. Using the vector

identity $\nabla \times \nabla \varphi = 0$, and since $\frac{\partial \varphi}{\partial x}$ and $\frac{\partial \varphi}{\partial y}$ are both zero, the vector identity reduces to:

$$\hat{x}\frac{\partial}{\partial y}(\frac{\partial \varphi}{\partial z}) + \hat{y}\frac{\partial}{\partial x}(\frac{\partial \varphi}{\partial z}) = 0 \tag{2.18}$$

This concludes that $\frac{\partial \varphi}{\partial z}$ doesn't vary with either x or y and therefore is constant over the cross sectional area of the m^{th} conductor. Hence:

$$\sigma \iint_{S_m} \frac{\partial \varphi}{\partial z} ds = \sigma \cdot S_m \frac{\partial \varphi}{\partial z} \tag{2.19}$$

where S_m is the cross sectional area of the m^{th} conductor. Combining (2.17) and (2.19) yields:

$$\frac{I_{0m}}{S_m} = -j\omega\sigma\vec{A}_m - \sigma\frac{\partial \varphi}{\partial z} \tag{2.20}$$

where I_{0m} is the total current flowing through the cross sectional area of the m^{th} conductor and $\vec{A}_m$ is the average magnetic potential of the m^{th} conductor. We can calculate $\frac{\partial \varphi}{\partial z}$ by rearranging (2.20) as

$$-\sigma\frac{\partial \varphi}{\partial z} = \frac{I_{0m}}{S_m} + j\omega\sigma\vec{A}_m \tag{2.21}$$

Combining (2.16) and (2.21) thus yields

$$\vec{J} = -j\omega\sigma\vec{A} + j\omega\sigma\vec{A}_m + \frac{I_{0m}}{S_m} \tag{2.22}$$

which is an integral equation for calculating the current distribution at any arbitrary point for any given current source.

Now in what follows, we simplify the solution by considering a system of infinitely long conductors along the *z*-direction in a homogenous, linear, isotropic medium.

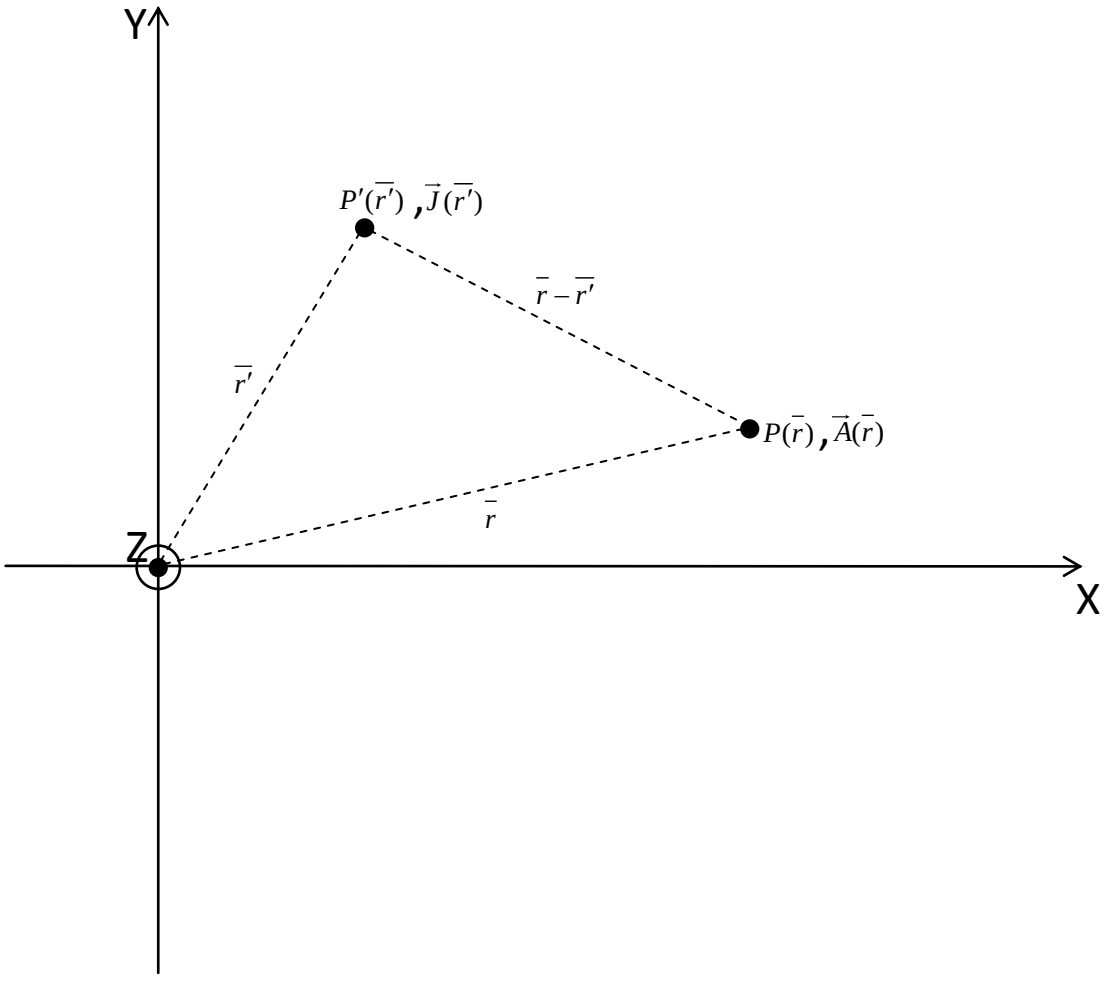

Figure 2.1 The point of observation with respect to the current source.

In Figure 2.1 the point of observation $\vec{r}$ and the current source position $\vec{r'}$ in the Cartesian coordinate system are defined as:

$$\vec{r} = x\hat{x} + y\hat{y} + z\hat{z} \tag{2.23}$$

$$\vec{r'} = x'\hat{x} + y'\hat{y} + z'\hat{z} \tag{2.24}$$

where $\hat{x}$, $\hat{y}$, and $\hat{z}$ are the unit vectors along the x, y, and z axes, respectively. Without loss of generality, we will assume that the observation point is positioned at $z = 0$. Therefore, we have:

$$\vec{r} - \vec{r'} = (x - x')\hat{x} + (y - y')\hat{y} + z'\hat{z} \tag{2.25}$$

Substituting (2.25) into (2.14) and applying the quasi-static condition for infinitely long conductors, we obtain:

$$A(x,y) = \frac{\mu_0}{4\pi}\iiint_V \frac{J(x',y')}{\sqrt{(x-x')^2 + (y-y')^2 + z'^2}}\,dx'dy'dz'$$

$$= \frac{\mu_0}{4\pi}\iint dx'dy'J(x',y')\int_{-\infty}^{+\infty}\frac{dz'}{\sqrt{(x-x')^2 + (y-y')^2 + z'^2}}$$

or

$$A(x,y) = \frac{\mu_0}{4\pi}\iint \ln[(x-x')^2 + (y-y')^2]J(x',y')dx'dy' \tag{2.26}$$

Equation (2.26) represents the vector magnetic potential of an infinite line in free space.

Next, we use image theory [4] to find the magnetic vector potential for the case where an infinite ground plane is present. This will allow us to include a reference ground plane into the system of transmission lines.

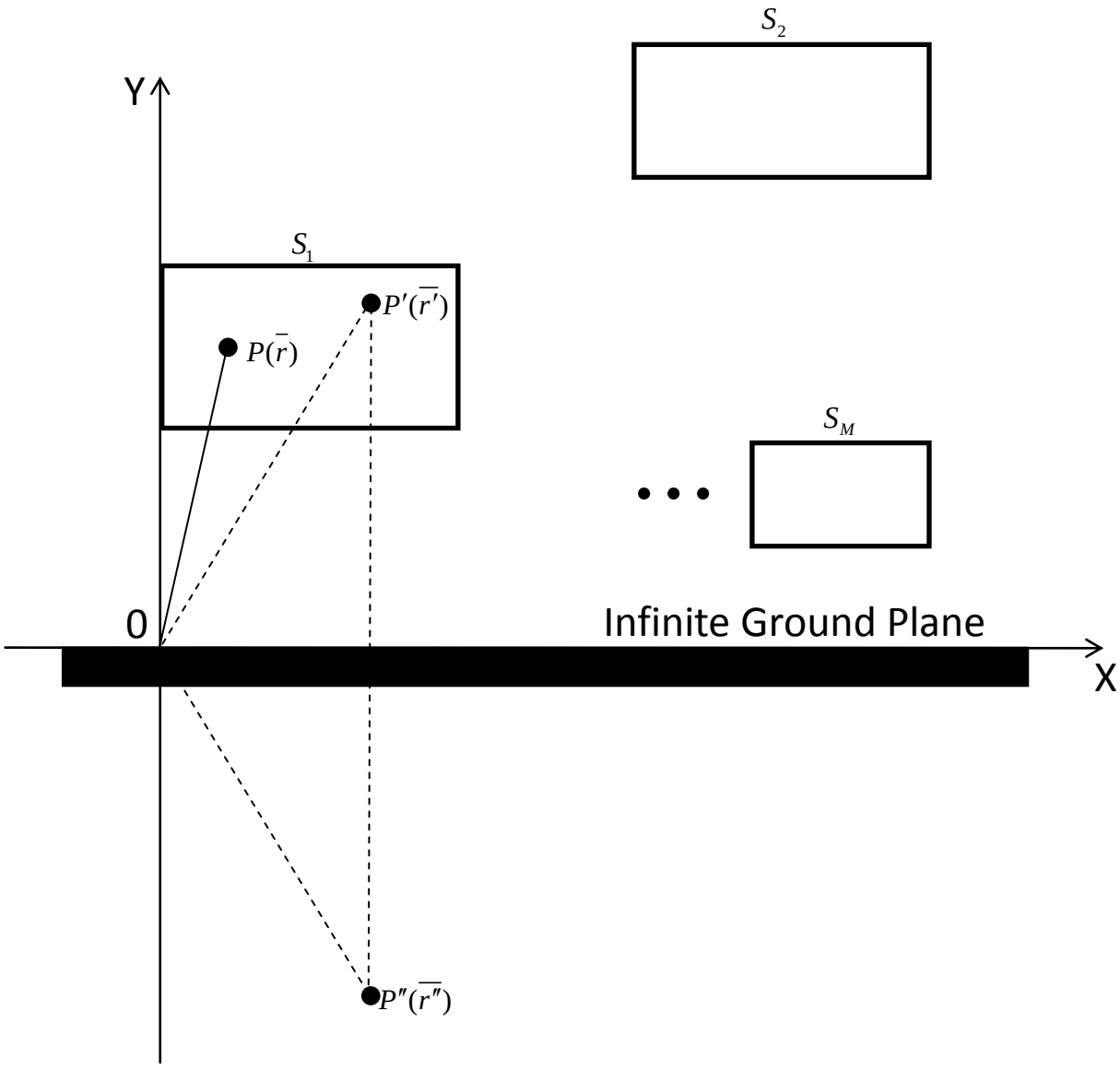

Figure 2.2 The method of images is used to include a reference ground plane into the system of transmission lines.

For simplicity we assume that there is only one ground plane that is located at $y = 0$ and is lossless and infinite in extent. The method of images involves eliminating the reference ground plane by adding in imaged conductors. These imaged conductors are situated at the same distance from the original ground plane and they carry currents with the same magnitudes in the opposite directions. The system of the conductors and its image create exactly the same fields in the region above the ground plane as the original system.

Figure 2.2 shows the observation point P, the source point P', and its image with respect to the ground plane, P''. The effective vector magnetic potential, $A(\vec{r})$, at point P, which is due to contributions from the two sources located at points $P'(\vec{r'})$ and $P''(\vec{r''})$, may be described by separately summing up the effect from each source

$$A(\vec{r}) = A_1(\vec{r}) + A_2(\vec{r}) \tag{2.27}$$

where $A_1(\vec{r})$ is due to the source at P' and $A_2(\vec{r})$ is due to the source at P''. Upon substituting $A_1(\vec{r})$ and $A_2(\vec{r})$ from (2.26) into (2.27), we get:

$$A(x,y) = \frac{\mu_0}{4\pi}\iint_S \ln[(x-x')^2 + (y-y')^2]J(x',y')dx'dy'$$

$$+ \frac{\mu_0}{4\pi}\iint_S \ln[(x-x'')^2 + (y-y'')^2]J(x'',y'')dx''dy'' \tag{2.28}$$

where $x' = x''$, $y' = y''$, $z' = z''$ and $J(x', y') = -J(x'', y'')$. Therefore (2.28) can be further simplified to:

$$A(x, y) = \frac{\mu_0}{4\pi} \iint_S J(x', y') G(x, y, x', y') dx' dy' \tag{2.29}$$

where $G(x, y, x', y')$ is the Green's function that is defined as

$$G(x, y, x', y') = \ln[\frac{(x-x')^2 + (y-y')^2}{(x-x')^2 + (y+y')^2}] \tag{2.30}$$

We now have an expression for the magnetic vector potential, $A(\vec{r})$, which is expressed in terms of the x and y locations and the source $J(\vec{r})$.

Finally, upon combining (2.29) and (2.22), we can calculate the current distribution at any point.

$$J(x, y) = \frac{j\omega\sigma\mu_0}{4\pi} \iint_{S_T} J(x', y') G(x, y, x', y') dx' dy' + \frac{I_{0m}}{S_m}$$

$$- \frac{j\omega\sigma\mu_0}{4\pi} \frac{1}{S_m} \iint_{S_m} [\iint_{S_T} J(x', y') G(x, y, x', y') dx' dy'] ds \tag{2.31}$$

where S_m is the cross-sectional area of the m^{th} conductor and $S_T = \sum_{i=1}^{M} S_i$ is the cross-sectional area of all conductors. Next, the current distribution in (2.31) is solved numerically and the per unit length resistance and inductance matrices of the conductors are calculated.

2.4 **Method of Moments**

From its early conception in the 1960's to the present, the method of moments (MOM) has been used in a variety of electromagnetic problems. In the area of electromagnetic compatibility, the method of moments has an advantage since it gives a direct and accurate solution for the current distribution. In this section, formulas will be given for the numerical calculation of the current distribution based on the MOM.

In order to solve for the current distribution for a system composed of *M* conductors, the conducting bodies are discretized using a piecewise constant expansion. For this purpose, the cross-sectional area of each conductor is discretized into smaller rectangular cells where the current is assumed to be constant over each section. If the discretization is sufficiently fine, then the distribution of the current will resemble the actual current distribution. Let's assign J_n to be the current of the n^{th} cell, then the total current can be expressed as

$$J(x,y) = \sum_{n=1}^{N} J_n C_n(x,y) \tag{2.32}$$

where $C_n(x,y)$ is a pulse function defined as:

$$C_n(x,y) = \begin{cases} 1 & \text{x and y is inside n}^{\text{th}}\text{ cell} \\ 0 & \text{elsewhere} \end{cases} \tag{2.33}$$

Here N is the total number of cells and can be stated in an alternate way by using the notation $N = \sum_{i=1}^{M} N_i$ where N_i is the number of cells for the i^{th} conductor and M is the number of conductors. Thus, there are N unknown constant coefficients, J_n in (2.32) which defines the current distribution at any point (x, y). Therefore, in order to find a unique solution, we need to have N linearly independent equations for J_n, $n = 1, \ldots, N$. These equations can be formed by combining (2.32) and(2.31):

$$\sum_{n=1}^{N} J_n C_n(x, y) - \frac{j\omega\sigma\mu_0}{4\pi} \sum_{n=1}^{N} (J_n \iint_{S_T} C_n(x', y') G(x, y, x', y') dx' dy'$$

$$+ \frac{j\omega\sigma\mu_0}{4\pi} \frac{1}{S_m} \iint_{S_m} \sum_{n=1}^{N} (J_n \iint_{S_T} C_n(x', y') G(x, y, x', y') dx' dy') ds = \frac{I_{0m}}{S_m} \qquad (2.34)$$

Let's set (x_i, y_i) to be the coordinates of the center of the i^{th} cell, where $i = 1, \ldots, N$. The resulting N equations will form a system of N independent equations with N unknowns: J_i, $i = 1, \ldots, N$. Therefore, it leads to a unique solution for the current of each cell, i.e.,

$$J_i - \frac{j\omega\sigma\mu_0}{4\pi} \sum_{n=1}^{N} (J_n \iint_{S_T} G(x_i, y_i, x', y') dx' dy')$$

$$+ \frac{j\omega\sigma\mu_0}{4\pi} \frac{1}{S_m} \iint_{S_m} \sum_{n=1}^{N} (J_n \iint_{S_T} G(x_i, y_i, x', y') dx' dy') ds = \frac{I_{0m}}{S_m} \qquad (2.35)$$

where S_m is the cross sectional area of the conductor that contains the i^{th} cell, S_T is the cross sectional area over all conductors, and I_{0m} is the total current flowing through the m^{th} conductor. (2.35) can also be stated in an alternate way by using the following notation

$$K_{in} = -\frac{j\omega\sigma\mu_0}{4\pi}\iint_{\Delta S_n} G(x_i, y_i, x', y')dx'dy' \tag{2.36}$$

Applying (2.36) to (2.35) we get

$$J_i + \sum_{n=1}^{N} J_n K_{in} - \frac{1}{S_m}\iint_{S_m}\sum_{n=1}^{N} J_n K_{\ln} ds = \frac{I_{0M}}{S_m} \tag{2.37}$$

which can be further simplified to:

$$J_i + \sum_{n=1}^{N} J_n K_{in} - \sum_{l}(\sum_{n=1}^{N} J_n K_{\ln}\frac{\Delta S_l}{S_m}) = \frac{I_{0M}}{S_m} \tag{2.38}$$

where $\sum_l \cdots$ denotes the integral term over the cross sectional area of the m^{th} conductor. By choosing $i = 1,\ldots,N$ in (2.38), a linear system of N equations is formed:

$i=1$: $\quad J_1 + (J_1K_{11} + J_2K_{12} + \cdots + J_NK_{1N})$

$$-(J_1\sum_l K_{l1}\frac{\Delta S_l}{S_m} + J_2\sum_l K_{l2}\frac{\Delta S_l}{S_m} + \cdots + J_N\sum_l K_{lN}\frac{\Delta S_l}{S_m}) = \frac{I_{01}}{S_1}$$

$i=2$: $\quad J_2 + (J_1K_{21} + J_2K_{22} + \cdots + J_NK_{2N})$

$$-(J_1\sum_l K_{l1}\frac{\Delta S_l}{S_m} + J_2\sum_l K_{l2}\frac{\Delta S_l}{S_m} + \cdots + J_N\sum_l K_{lN}\frac{\Delta S_l}{S_m}) = \frac{I_{01}}{S_1}$$

$\vdots$

$$i = N: \quad J_N + (J_1 K_{N1} + J_2 K_{N2} + \cdots + J_N K_{NN})$$

$$-(J_1 \sum_l K_{l1} \frac{\Delta S_l}{S_m} + J_2 \sum_l K_{l2} \frac{\Delta S_l}{S_m} + \cdots + J_N \sum_l K_{lN} \frac{\Delta S_l}{S_m}) = \frac{I_{0m}}{S_m}$$

This system of equations can be expressed in matrix form as:

$$[Z] \cdot [J] = [B] \tag{2.39}$$

Where $[Z]$ is a $N \times N$ matrix and $[J]$ and $[B]$ are $N \times 1$ matrices that are defined as:

$$Z = \begin{bmatrix} [Z_{11}] & [Z_{12}] & \cdots & [Z_{1M}] \\ [Z_{21}] & [Z_{22}] & \cdots & [Z_{2M}] \\ \vdots & \vdots & \ddots & \vdots \\ [Z_{M1}] & [Z_{M2}] & \cdots & [Z_{MM}] \end{bmatrix}$$

$$[J] = \begin{bmatrix} [J_1] \\ [J_2] \\ \vdots \\ [J_M] \end{bmatrix}$$

$$[B] = \begin{bmatrix} [B_1] \\ [B_2] \\ \vdots \\ [B_M] \end{bmatrix}$$

From (2.39), the current vector, $[J]$, can be calculated from

$$[J]=[Z]^{-1}[B] \tag{2.40}$$

2.5 Inductance and Resistance Matrices

In section 2.2 we found an analytical solution for the magnetic vector potential, $\vec{A}(\vec{r})$, and the current density vector, $\vec{J}(\vec{r})$, for a system of coupled conductors above an infinite ground plane. In this section, we are now going to find an analytical solution for the per unit length (p.u.l.) inductance and resistance matrices in terms of $\vec{A}(\vec{r})$ and $\vec{J}(\vec{r})$. We begin with the definition for the time average magnetic energy, U_m, in a steady state situation

$$U_m=\frac{1}{4}\mathrm{Re}\int_{S_T}\vec{J}\cdot\vec{A}ds \tag{2.41}$$

where S_T is the cross sectional area over all conductors. The time average magnetic energy, U_m, can be expressed in an alternate way by using the conductor's mutual and self inductance terms as:

$$U_m=\frac{1}{4}\sum_i\sum_j L_{ij}I_iI_j \tag{2.42}$$

where L_{ij} for $i,j=1,2,\cdots,N$ are the mutual inductances ($i\neq j$), and the self inductances ($i=j$) of the conductors, respectively. In order to calculate the self inductance of the i^{th} conductor, L_{ii}, we need to set I_j, $j=1,2,\cdots,N$ ($j\neq i$) to zero and calculate the stored magnetic energy, U_m^{ii}, as

$$U_m^{ii} = \frac{1}{4} L_{ii} I_i^2 \tag{2.43}$$

Enforcing the condition where $I_j = 0$, $j = 1, 2, \cdots, N$ ($j \neq i$) in (2.41) and combining the results with (2.43) yields

$$L_{ii} = \frac{\mathrm{Re}[\int_{\Delta S_i} \vec{J}_i^* \cdot \vec{A}_i \, ds]}{I_i^2} \tag{2.44}$$

where $\vec{A}_i$ is the vector magnetic potential at the point (x_i, y_i), which is the center of the i^{th} cell.

In a similar fashion, the mutual inductance terms can be calculated by driving conductors i and j with currents I_i and I_j, respectively, and setting I_k, $k = 1, 2, \cdots, N$, ($k \neq i$ and $k \neq j$) to zero. Therefore, we get

$$U_m^{ij} = \frac{1}{2} L_{ij} I_i I_j + \frac{1}{4} L_{ii} I_i^2 + \frac{1}{4} L_{jj} I_j^2 \tag{2.45}$$

Combining (2.43) with (2.45) and rearranging the terms leads to

$$L_{ij} = 2 \frac{U_m^{ij} - U_m^{ii} - U_m^{jj}}{I_i I_j} \tag{2.46}$$

An alternative way to express U_m^{ij} using (2.41) is

$$U_m^{ij} = \frac{1}{4}\mathrm{Re}\int_{\Delta S_i + \Delta S_j} \vec{J}_i^{\,*}\vec{A}_j ds \tag{2.47}$$

Combining (2.43) and (2.46) yields

$$L_{ij} = \frac{\mathrm{Re}[\int_{\Delta S_i \Delta S_j} \vec{J}_i^{\,*}\vec{A}_j ds - 2\int_{\Delta S_i} \vec{J}_i^{\,*}\cdot\vec{A}_i\, ds - 2\int_{\Delta S_j} \vec{J}_j^{\,*}\cdot\vec{A}_j\, ds]}{2I_i I_j} \tag{2.48}$$

Next we calculate the per-unit-length resistance of the conductors. For this purpose, we use the time average power dissipation which is given by

$$P_{av} = \frac{1}{2}\mathrm{Re}\int_{S_T} \vec{J}\cdot\vec{E}^{\,*} ds \tag{2.49}$$

The time average power dissipation, P_{av}, may be stated in an alternate way as

$$P_{av} = \frac{1}{2}\mathrm{Re}\left|I^2\right| \tag{2.50}$$

Since $I = \int_S Jds$, we have

$$P_{av} = \frac{1}{2}\mathrm{Re}\left|\int_S Jds\right|^2 \tag{2.51}$$

Combining (2.49) and (2.51) with the fact that $\bar{J} = \sigma\bar{E}$ we get

$$R_{ii} = \frac{1}{\sigma_i} \frac{\int_{\Delta S_i} |J_i|^2 \, ds}{\left| \int_{\Delta S_i} J_i ds \right|^2} \tag{2.52}$$

$$R_{ij} = \frac{1}{\sigma_i} \frac{\int_{\Delta S_i} |J_i|^2 \, ds}{\left| \int_{\Delta S_j} J_j ds \right|^2} \tag{2.53}$$

where σ_i is the metal conductivity of the i^{th} conductor, R_{ii} is the per unit length resistance of the i^{th} conductor due to its own current, and R_{ij} is the per unit length resistance of the i^{th} conductor due to the current in the j^{th} conductor.

CHAPTER 3 NEW EFFICIENT AND PASSIVE MULTI-CONDUCTOR TRANSMISSION LINE MODEL

3.1 Introduction

Accurate electromagnetic modeling of multiple-level interconnections is essential for signal integrity assessment. Of particular interest is the development of robust models for high-speed interconnections that are modeled as multi-conductor transmission lines (MTL). The most popular approach for discrete modeling of interconnects uses a direct segmentation of the line into sections of length Δz, which are chosen to be a small fraction of the wavelength. Then, for the case of a simple, two-conductor transmission line, each segment is replaced by a lumped-element circuit model with series elements $L(z)\cdot\Delta z$, $R(z)\cdot\Delta z$, and shunt elements $G(z)\cdot\Delta z$, $C(z)\cdot\Delta z$, where $L(z)$, $R(z)$, $C(z)$, and $G(z)$ are the per-unit-length (p.u.l.) inductance, resistance, capacitance and conductance of the line. For the case of an MTL, it is the p.u.l. inductance, resistance, capacitance and conductance matrices L, R, C, and G, that are used for the development of the lumped circuit.

Despite its simplicity, this approach has the disadvantage that the choice of Δz depends not only on the minimum wavelength of interest (or, equivalently, to the pulse bandwidth), but also on the electrical length of the interconnect (i.e. its length in

wavelengths) [5]. The consequence of this is that, for accurate simulation of the propagation of multi-GHz bandwidth pulses, the number of segments per minimum wavelength is about 20. To illustrate the significance of this, consider a pulse of rise time $\tau_r = 20$ ps. An approximate bandwidth for such a pulse is $BW \sim 0.3/\tau_r = 15$ GHz. Assuming an insulating medium with relative dielectric constant of 4, the minimum wavelength that needs to be resolved is found to be 1 cm. Consequently, for a 3 cm-long interconnect, 60 segments are required for the accurate representation of a propagating pulse with a 20 ps rise time. Clearly, such a large number of segments is undesirable, since it results in a very large numbers of lumped elements, especially when buses involving tens of coupled interconnects need to be modeled.

In this chapter, a new discrete model for MTL systems will be proposed that takes advantage of the high accuracy of compact differences to reduce the number of degrees of freedom per minimum wavelength to one third of that used in the segmentation approach. Furthermore, the proposed discrete model is passive, and compatible with PRIMA (Passive Reduce-Order Interconnect Macromodeling Algorithm).

3.2 The Semi-Discrete Interconnect Model

We begin with the development of the discritization process. For the sake of clarity, and without loss of generality, the mathematical development is given for the simple case of a two-conductor transmission line with one of the conductors taken as reference. The extension to the multi-conductor interconnect case is rather straightforward, and all results derived for the two-conductor transmission line apply

directly to the multi-conductor case. For the purposes of this development the per unit length (p.u.l) parameters of the interconnect are assumed to be independent of frequency. However, they are allowed to be position dependent. Later in the next chapter, we extend the model to MTL systems with frequency dependent parameters. With the aforementioned conditions, the governing Telegrapher's equations for the voltage, $V(z,s)$, and the current, $I(z,s)$, on an interconnect of length l in the Laplace domain will assume the forms:

$$\frac{d}{dz}V(z,s) = -(R(z) + sL(z))I(z,s) - f_v \tag{3.1}$$

$$\frac{d}{dz}I(z,s) = -(G(z) + sC(z))V(z,s) - f_I \tag{3.2}$$

where s is the Laplace transform variable, and $R(z)$, $L(z)$, $G(z)$, $C(z)$ are the p.u.l resistance, inductance, conductance and capacitance of the interconnect, respectively. The forcing terms f_V and f_I represent any distributed source along the line. For the case of macromodeling, they reduce to appropriate boundary conditions at the two end of the line involving port voltages and/or currents.

The spatial discretization of these equations can be affected in several ways. The most popular one is the direct segmentation of the transmission line into sections of length Δz, chosen to be a small fraction of the wavelength. However, as explained in section 3.1, this straightforward approach is undesirable since it results in a very large number of lumped circuit elements, especially when dealing with multi-conductor interconnects. More efficient alternatives to the segmentation approach are available. One specific approach utilizes the exponential convergence of Chebyshev

interpolation to achieve highly accurate approximations using at most four degrees of freedom per wavelength [6], [7].

We will return to the specifics of the process used for the discretization of the spatial derivatives in (3.1) and (3.2) when the issue of passivity is discussed. At this point, it suffices to assume that a specific discretization process has been selected, where the lines ($0 \le z \le l$) are segmented into M_z sections, $z_1, ..., z_{M_z}$ and the line voltages and currents are approximated as:

$$V(z,s) = \sum_{m=1}^{M_z} V_m(s) P_m(z) \tag{3.3}$$

$$I(z,s) = \sum_{m=1}^{M_z} I_m(s) Q_m(z) \tag{3.4}$$

where $V_m(s) = V(z_m, s)$, $I_m(s) = I(z_m, s)$, $m = 1, 2, ..., M_z$ are the degrees of freedom of the approximation, while $P_m(z)$, $Q_m(z)$, are known, expansion functions. Upon substituting (3.3) and (3.4) into (3.1) and (3.2) we get:

$$\sum_{m=1}^{M_z} V_m(s) \frac{dP_m(z)}{dz} = -(R(z) + sL(z)) \sum_{m=1}^{M_z} I_m(s) Q_m(z) - f_v \tag{3.5}$$

$$\sum_{m=1}^{M_z} I_m(s) \frac{dQ_m(z)}{dz} = -(G(z) + sC(z)) \sum_{m=1}^{M_z} V_m(s) P_m(z) - f \tag{3.6}$$

By forcing the equations (3.5) and (3.6) to be satisfied at the points $z = z_i$, $i = 1, 2, ..., M_z$, we find that

$$\sum_{m=1}^{M_z} V_m(s) D_{V_{mi}} = -(R(z_i) + sL(z_i)) I_i(s) - f_v \tag{3.7}$$

$$\sum_{m=1}^{M_z} I_m(s) D_{I_{mi}} = -(G(z_i) + sC(z_i)) V_i(s) - f_I \tag{3.8}$$

where $D_{V_{mi}} = \left.\frac{dP_m(z)}{dz}\right|_{z=z_i}$ and $D_{I_{mi}} = \left.\frac{dQ_m(z)}{dz}\right|_{z=z_i}$. The system of equations in (3.7) and (3.8) may now be cast in a discrete matrix system of the form:

$$\begin{bmatrix} R_d & D_V \\ D_I & G_d \end{bmatrix} \begin{bmatrix} I \\ V \end{bmatrix} + s \begin{bmatrix} L_d & 0 \\ 0 & C_d \end{bmatrix} \begin{bmatrix} I \\ V \end{bmatrix} = \begin{bmatrix} f_V \\ f_I \end{bmatrix} \tag{3.9}$$

where the vectors I and V of length M_z contain the coefficients in the expansions (3.7) and (3.8):

$$\begin{bmatrix} I \\ V \end{bmatrix} = \begin{bmatrix} I_1 & \dots & I_{M_z} & V_1 & \dots & V_{M_z} \end{bmatrix}^T \tag{3.10}$$

The matrices D_V and D_I are the discrete approximation of the spatial derivatives of the line voltage and current distributions, respectively; the matrices R_d, G_d, L_d, C_d are the resulting discrete approximations of the p.u.l. parameters of the line, consistent with the choice of the expansion functions in (3.3) and (3.4), and the testing process:

$$R_d = diag\left\{R(z_1) \quad ... \quad R(z_{M_z})\right\} \tag{3.11}$$

$$G_d = diag\left\{G(z_1) \quad ... \quad G(z_{M_z})\right\} \tag{3.12}$$

$$L_d = diag\left\{L(z_1) \quad ... \quad L(z_{M_z})\right\} \tag{3.13}$$

$$C_d = diag\left\{C(z_1) \quad ... \quad C(z_{M_z})\right\} \tag{3.14}$$

Because of the passivity of the media, the matrices R_d and G_d are (symmetric) non-negative definite. For the case of a multi-conductor line, the symmetry of these matrices is maintained due to reciprocity. The matrices L_d and C_d are also symmetric and non-negative definite [8]. It is important that these properties are preserved during the discretization process. Later in this chapter, we will show that such conditions are required to ensure the passivity of the system. Finally, the vectors f_V and f_I are the discrete forms of the source terms in (3.1) and (3.2). More specifically, it is assumed that the port voltages are specified at the two end points of the line. Consequently, in (3.9) only f_V is nonzero and more specifically, it's only nonzero entries are its first and last elements. Since the objective is the development of reduced-order models for the admittance matrix elements of the two-port system that will represent the two-conductor line, it is convenient to rewrite the source term in (3.9) in the following fashion:

$$\begin{bmatrix} 1 & 0 & ... & 0 & 0 & 0 & ... & 0 \\ 0 & 0 & ... & 0 & -1 & 0 & ... & 0 \end{bmatrix}^T \begin{bmatrix} V_A \\ V_B \end{bmatrix} = FV_p \tag{3.15}$$

where the dimension of F is $2M_z \times 2$ and the rows with the non-zero entries are 1 and M_z. The desired outputs are the currents at the two end points (ports). Thus, the two-element output vector I_P is written in terms of the state vector of the unknowns as:

$$I_P = F^T \begin{bmatrix} I \\ V \end{bmatrix} \tag{3.16}$$

A more compact form of the discrete system can be obtained by introducing the notation:

$$X^T = \begin{bmatrix} I \\ V \end{bmatrix} \tag{3.17}$$

$$P = \begin{bmatrix} R_d & D_V \\ D_I & G_d \end{bmatrix} \tag{3.18}$$

$$Q = \begin{bmatrix} L_d & 0 \\ 0 & C_d \end{bmatrix} \tag{3.19}$$

Thus, (3.9) and (3.16) maybe cast in the form:

$$(P + sQ)X(s) = FV_P(s) \tag{3.20}$$

$$I_P(s) = F^T X(s) \tag{3.21}$$

From (3.20) and (3.21), the admittance matrix is given by:

$$Y(s) = F^T (P + sQ)^{-1} F \tag{3.22}$$

From (3.22), it is clear that the eigenvalues of $P^{-1}Q$ correspond to the poles of the admittance matrix $Y(s)$.

The objective of model order reduction is to generate rational-function approximations to the elements of $Y(s)$ with an order much smaller than the order of the discrete system, $2M_z$. At this point, it is appropriate to consider this approximation objective carefully in view of the fact that what is of primary interest in the context of this discussion is the model order reduction of a distributed electromagnetic systems, i.e., a system that exhibits time retardation. Continuous, distributed electromagnetic systems are, of course, of infinite order; hence, the number of poles required for the exact representation of their delay properties is infinite. However, when dealing with a numerical approximation of Maxwell's equation in general, and for this specific case the system of Telegrapher's equations, what is of interest is the reduced-order modeling of the resulting discrete electromagnetic system. These discrete systems have finite order, and their transfer functions have finite bandwidth, which is controlled by the grid size and the order of approximation of the spatial derivatives. Consequently, the pole-residue representation of the transfer function of the approximated electromagnetic system will be of finite order.

The PRIMA algorithm has been shown to lead to guaranteed passive-order models for the case of RLC networks [2]. It will be shown here that this algorithm is also suitable for passive model order reduction of interconnect networks. However, it

is premature to talk about passivity of reduced-order model without investigating the passivity of the original discrete model that results from the discretization of Telegrapher's equations. Furthermore, it is more efficient to start with an original discrete model that has a smaller order of freedom without the loss of accuracy. Development of such a model is the topic of the next section.

3.3 The Use of Compact Differences

In this section a high order compact central difference scheme is applied in the discretization process to numerically calculate the spatial partial differences in Telegraphers' equations. The high order accuracy of the compact difference approximations of the spatial derivatives leads to a very accurate, broadband (multi GHz), discrete interconnect model with a number of degrees of freedom much smaller than the one required when a standard second order-accurate finite difference approximation (e.g. the commonly used cascaded lumped RLC-circuit modeling of interconnects) is used. This facilitates the computational efficiency of the model order reduction process and allows for enhanced accuracy. The details of the theory of compact difference operators and the details of their application to the discretization of wave equations can be found in [9]. The emphasis here is placed on the specifics of their implementation for the approximation of the spatial derivatives of the transmission line voltage and current.

In numerical calculations of the finite difference, the values of a function on a set of nodes are given. Then the finite difference approximation to the derivative of the function is expressed as a linear combination of the given function values. The

development begins with discretization of the transmission line into M_z segments of equal lengths Δz. The unknown voltage, $V(z)$, is defined in terms of its values at the nodes $z = i(\Delta z)$, $i = 0,1,2,\ldots,M_z$. The current distribution, $I(z)$, is described in terms of its values, I_0 and I_M at the two end points, as well as its values at the centers of the M_z segments, $z = (i-1/2)\cdot(\Delta z)$, $i = 0,1,2,\ldots,M_z$. The approximation of the spatial derivatives in Telegrapher's equations is effected by using the following compact central operator:

$$\alpha_1 \left.\frac{\partial f}{\partial z}\right|_{i+1} + \alpha_2 \left.\frac{\partial f}{\partial z}\right|_{i} + \alpha_1 \left.\frac{\partial f}{\partial z}\right|_{i-1} = \frac{f_{i+1/2} - f_{i-1/2}}{\Delta z} \tag{3.23}$$

where $f(z)$ stands for either $V(z)$ or $I(z)$ and i denotes the node where the operator is centered. The relationships between the coefficients α_1 and α_2 are derived by matching the Taylor series coefficients of the same order. Here the order of accuracy is chosen to be of 4^{th} order. The first unmatched coefficient determines the formal truncation error of the approximation (3.23). These constraints for fourth order accuracy are:

$$\frac{1}{\alpha_2} = 1 + 2\frac{\alpha_1}{\alpha_2} \tag{3.24}$$

$$\frac{1}{\alpha_2} = 2\frac{3!}{2!}(2^2\frac{\alpha_1}{\alpha_2}) \tag{3.25}$$

From (3.24) and (3.25), coefficients are calculated as $\alpha_1 = 1/24$ and $\alpha_2 = 11/12$. If this discretization operation is applied to the voltage and current nodes, we get:

$$\alpha_1 \left.\frac{\partial V}{\partial z}\right|_{k+1} + \alpha_2 \left.\frac{\partial V}{\partial z}\right|_{k} + \alpha_1 \left.\frac{\partial V}{\partial z}\right|_{k-1} = \frac{V_{k+1/2} - V_{k-1/2}}{\Delta z} \tag{3.26}$$

$$\alpha_1 \left.\frac{\partial I}{\partial z}\right|_{k+1} + \alpha_2 \left.\frac{\partial I}{\partial z}\right|_{k} + \alpha_1 \left.\frac{\partial I}{\partial z}\right|_{k-1} = \frac{I_{k+1/2} - I_{k-1/2}}{\Delta z} \tag{3.27}$$

Calculating (3.26) and (3.27) at internal points, k, equal to $i+3/2$, $i+1/2$, $i-1/2$ and applying it to the Telegrapher's equations in (3.1) and (3.25) produces discrete forms of the equations

$$-\alpha_1 Z_{i+3/2} I_{i+3/2} - \alpha_2 Z_{i+1/2} I_{i+1/2} - \alpha_1 Z_{i-1/2} I_{i-1/2} = \frac{V_{i+1} - V_i}{\Delta z} \qquad i = 1, 2, ..., M_z - 2 \tag{3.28}$$

$$-\alpha_1 Y_{i+1} V_{i+1} - \alpha_2 Y_i V_i - \alpha_1 Y_{i-1} V_{i-1} = \frac{I_{i+1/2} - I_{i-1/2}}{\Delta z} \qquad i = 1, 2, ..., M_z - 1 \tag{3.29}$$

where $Z_i = R(i.\Delta z) + sL(i.\Delta z)$, $Y_i = G(i.\Delta z) + sC(i.\Delta z)$.

Clearly, (3.23) cannot be used at the nodes at the end points of the transmission line. Instead, second-order compact difference operators are used. More specifically, for the left end-point of the line, use is made of the following forward second-order schemes:

$$\alpha_3 \left.\frac{\partial f}{\partial z}\right|_{i} + \alpha_1 \left.\frac{\partial f}{\partial z}\right|_{i+1} = \frac{f_{i+1/2} - f_{i-1/2}}{\Delta z} \tag{3.30}$$

$$\alpha_4 \left.\frac{\partial f}{\partial z}\right|_{i} + \alpha_1 \left.\frac{\partial f}{\partial z}\right|_{i+1} = \frac{f_{i+1/2} - f_i}{\Delta z} \tag{3.31}$$

where $\alpha_3 = 1 - \alpha_1$ and $\alpha_4 = \frac{1}{2} - \alpha_1$. On the other hand, second-order backward schemes are implemented at the right end-point of the line:

$$\alpha_3 \left.\frac{\partial f}{\partial z}\right|_i + \alpha_1 \left.\frac{\partial f}{\partial z}\right|_{i-1} = \frac{f_{i+1/2} - f_{i-1/2}}{\Delta z} \tag{3.32}$$

$$\alpha_4 \left.\frac{\partial f}{\partial z}\right|_i + \alpha_1 \left.\frac{\partial f}{\partial z}\right|_{i-1} = \frac{f_i - f_{i-1/2}}{\Delta z} \tag{3.33}$$

Using (3.30), (3.31), (3.32), and (3.33)with (3.1) and (3.2), the following discrete equations are obtained for the nodes at the end-points of the line:

$$-\alpha_3 Z_{1/2} I_{1/2} - \alpha_1 Z_{3/2} I_{3/2} = \frac{V_1 - V_0}{\Delta z} \tag{3.34}$$

$$-\alpha_4 Y_0 V_0 - \alpha_1 Y_1 V_1 = \frac{I_{1/2} - I_0}{\Delta z} \tag{3.35}$$

$$-\alpha_3 Z_{M_z - 1/2} I_{M_z - 1/2} - \alpha_1 Z_{M_z - 3/2} I_{M_z - 3/2} = \frac{V_{M_z} - V_{M_z - 1}}{\Delta z} \tag{3.36}$$

$$-\alpha_4 Y_{M_z} V_{M_z} - \alpha_1 Y_{M_z - 1} V_{M_z - 1} = \frac{I_{M_z} - I_{M_z - 1/2}}{\Delta z} \tag{3.37}$$

The $2M_z + 1$ coupled equations described by (3.28), (3.29) and (3.19)-(3.22) need to be complemented by the boundary conditions at the end points, namely, $V_0 = V_A$ and

$V_{M_z} = V_B$, where V_A and V_B are the near-end and far-end voltages of the transmission line, respectively. The resulting system may be cast in matrix form as follows:

$$\underbrace{\begin{bmatrix} R_d + sL_d & D_V \\ D_I & G_d + sC_d \end{bmatrix}}_{P+sQ} \underbrace{\begin{bmatrix} I_0(s) \\ I_t(s) \\ I_{M_z}(s) \\ V_t(s) \end{bmatrix}}_{X_T} + \begin{bmatrix} -V_A \\ 0 \\ \vdots \\ 0 \\ V_B \\ 0 \\ \vdots \\ 0 \end{bmatrix} = 0 \tag{3.38}$$

where

$$R_d + sL_d = \begin{bmatrix} 0 & 0 & 0 & & \cdots & & 0 \\ 0 & a_3 & a_1 & & & & \vdots \\ 0 & a_1 & a_2 & \ddots & & & \vdots \\ \vdots & & \ddots & \ddots & & & \\ \vdots & & & \ddots & a_2 & a_1 & 0 \\ & & & & a_1 & a_3 & 0 \\ 0 & \cdots & & & 0 & 0 & 0 \end{bmatrix} \tag{3.39}$$

$$D_V = \begin{bmatrix} 1 & & & & & \\ -1 & 1 & & & & \\ & -1 & & & & \\ & & \ddots & \ddots & & \\ & & & & 1 & \\ & & & & -1 & \end{bmatrix} \tag{3.40}$$

$$D_I = \begin{bmatrix} -1 & 1 & & & \\ & -1 & 1 & & \\ & & \ddots & \ddots & \\ & & & -1 & 1 \end{bmatrix} \tag{3.41}$$

$$G_d + sC_d = \begin{bmatrix} A_4 & A_1 & & & \\ A_1 & A_2 & \ddots & & \\ & \ddots & \ddots & \ddots & \\ & & \ddots & A_2 & A_1 \\ & & & A_1 & A_4 \end{bmatrix} \tag{3.42}$$

$a_i = \alpha_i Z(j \cdot \Delta z) \cdot \Delta z$, $i = 1,2,3$, j =Column Number in (3.39)

$A_i = \alpha_i Y(j \cdot \Delta z) \cdot \Delta z$, $i = 1,2,4$, j =Column Number in (3.42)

$$I_t(s) = \begin{bmatrix} I_{1/2}(s) \\ I_{3/2}(s) \\ \vdots \\ I_{M_z - 1/2}(s) \end{bmatrix}$$

$$V_t(s) = \begin{bmatrix} V_0(s) \\ V_1(s) \\ \vdots \\ V_{M_z}(s) \end{bmatrix}$$

Next we introduce the selection matrix, F

$$F = \begin{bmatrix} 1 & 0 \\ 0 & 0 \\ \vdots & \vdots \\ 0 & 0 \\ 0 & -1 \\ 0 & 0 \\ \vdots & \vdots \\ 0 & 0 \end{bmatrix} \tag{3.43}$$

in order to relate the port current to the state vector, X_T, as

$$\begin{bmatrix} I_A \\ I_B \end{bmatrix} = F^T X_T \tag{3.44}$$

where I_A and I_B are current at the two ports, i.e., $I_A = I_0$, $I_B = -I_{M_z}$. We also have the following relation between the selection matrix, F, and the port voltages, V_A and V_B:

$$\begin{bmatrix} -V_A \\ 0 \\ \vdots \\ 0 \\ V_B \\ 0 \\ \vdots \\ 0 \end{bmatrix} = -F \begin{bmatrix} V_A \\ V_B \end{bmatrix} \tag{3.45}$$

Using the above relations, one can rewrite (3.38) in the following form:

$$(P + sQ) X_T = F \begin{bmatrix} V_A \\ V_B \end{bmatrix} \tag{3.46}$$

$$\begin{bmatrix} I_A \\ I_B \end{bmatrix} = F^T X_T \tag{3.47}$$

The use of the fourth-order accurate compact difference operator leads to very accurate transient simulations as will be demonstrated later in the numerical experiments. This accuracy is achieved despite utilizing only 8.2 degrees of freedom per minimum wavelength, which is at least a three-fold reduction in the dimension of the matrices when compared to direct segmentation. This provides a significant computational advantage when model order reduction algorithms are applied.

However, in order for the discrete model to be suitable for passive model order reduction algorithms, it must be passive. Next, the discrete model in (3.46) and (3.47) will be examined for passivity conditions.

3.4 **Passivity of the Discrete Transmission Line**

The analysis of the passivity of the discrete model of (3.46) and (3.47) will make use of the following results [10]:

Theorem 1: The transfer function matrix $H(s)$ of a passive (linear, solvable, time-invariant) network is positive-real; that is,

a) Each element of $H(s)$ is analytic for $\mathrm{Re}\{s\} > 0$.

b) $H(s^*) = H^*(s)$ for $\mathrm{Re}\{s\} > 0$.

c) $H_h(s) = (H^*)^T(s) + H(s) \geq 0$ for $\mathrm{Re}\{s\} > 0$.

Theorem 2: If a matrix, A, is positive-real, then so is its inverse, if it exists.

Theorem 3: If A is positive-real and $A_h > 0$ for $\mathrm{Re}\{s\} > 0$, then A^{-1} exists.

Theorem 4: If F is a real, constant, $m \times n$ matrix and A is an $m \times m$ positive-real matrix, then the matrix $F^T A F$ is an $n \times n$ positive-real matrix.

Consider the transfer function matrix (or, more specifically, the admittance matrix) of the system given in (3.22) that is based on the transmission line system model in (3.46) and (3.47). According to *Theorem 1*, the discrete approximation to Telegrapher's equations will be passive if Y is positive-real. However, the matrix F in (3.46) and (3.47) is a real constant matrix. Thus, in view of *Theorems 2*, *3*, and *4*, to prove the passivity of the discrete system of (3.46) and (3.47) it suffices to show that

the matrix $W = P + sQ$ is positive-real and $W_h(s) > 0$ for $\mathrm{Re}\{s\} > 0$. This takes us back to *Theorem 1* where the three requirements for a matrix to be positive real are given. First, we note that matrices P and Q are real. Hence, requirements (a) and (b) are automatically satisfied. To prove that requirement (c) is also satisfied and, moreover, $W_h(s) > 0$, we need to show that $(Z^*)^T W_h Z > 0$ for $\mathrm{Re}\{s\} > 0$ and for any complex vector Z. Setting $s = \alpha + j\omega$, one obtains after some straightforward matrix algebra:

$$(Z^*)^T W_h Z = (Z^*)^T [(P + P^T) + 2\alpha Q] Z \tag{3.48}$$

where use has been made of the fact that P and Q are real matrices and Q is symmetric. Let's assume for now that R_d, L_d, G_d and C_d in (3.39) and (3.42) are positive definite matrices. Therefore, it follows that Q is a positive definite matrix and thus $2\alpha(Z^*)^T QZ > 0$ for $\alpha > 0$. The remaining term in (3.48)involves the sum $P + P^T$. From (3.48) it is given by:

$$P + P^T = \begin{bmatrix} 2R_d & D_V + D_I{}^T \\ (D_V + D_I{}^T)^T & 2G_d \end{bmatrix} \tag{3.49}$$

where use has been made of the fact that R_d and G_d are symmetric. Assuming that R_d and G_d are positive definite matrices, it becomes apparent that the specific form of the numerical approximation of the two derivative operators in Telegrapher's equations plays an important role on the passivity of the approximation. To

elaborate, let us expand the term $(Z^*)^T(P+P^T)Z$, with Z written in the form of: $Z=\begin{bmatrix}V & W\end{bmatrix}^T$. Through some straightforward matrix algebra one obtains:

$$\begin{aligned}(Z^*)^T(P+P^T)Z &= 2((V^*)^T R_d V)+ \\ 2((W^*)^T G_d W)+((V^*)^T(D_V+D_I^T)W)+&[((V^*)^T(D_V+D_I^T)W)^*]^T\end{aligned} \tag{3.50}$$

The passivity of the numerical model will depend on the positive-definite or non-negative-definite condition of each of the four terms in (3.50). The last two terms in (3.50) are non-negative definite for any Z if:

$$D_V=-D_I^T \tag{3.51}$$

From (3.40) and (3.41), it is obvious that the condition in (3.51) is met for the discrete transmission model using fourth order compact differences. In general, any discretization process that leads to positive definite R_d and G_d matrices and a matrix representation of the spatial derivatives in Telegrapher's equation that satisfy (3.51) will lead to a guaranteed-passive discrete model. Now, what remains is to show that the first two terms in (3.50) are positive definite for the discrete model using fourth order compact differences in (3.39) and (3.42). Let us start with R_d and expand the first term in (3.50) using its matrix definition in (3.39)

$$(V^*)^T R_d V = \begin{bmatrix} v_0^* & v_1^* & v_2^* & v_3^* & \cdots & v_{M_z}^* \end{bmatrix} \begin{bmatrix} 0 & 0 & 0 & \cdots & & & 0 \\ 0 & \gamma_3 & \gamma_1 & 0 & \cdots & & 0 \\ 0 & \gamma_1 & \gamma_2 & \gamma_1 & 0 & \cdots & 0 \\ \vdots & & \ddots & \ddots & \ddots & & \vdots \\ 0 & \cdots & 0 & \gamma_1 & \gamma_2 & \gamma_1 & 0 \\ 0 & & \cdots & 0 & \gamma_1 & \gamma_3 & 0 \\ 0 & & \cdots & 0 & 0 & 0 & 0 \end{bmatrix} \begin{bmatrix} v_0 \\ v_1 \\ v_2 \\ v_3 \\ \vdots \\ v_{M_z} \end{bmatrix} \quad (3.52)$$

where $V = \begin{bmatrix} v_0 & v_1 & v_2 & v_3 & \cdots & v_{M_z} \end{bmatrix}^T$ is an arbitrary constant $M_z \times 1$ vector and $\gamma_i = \mathrm{Re}\{a_i\}$, $i = 1,2,3$. We can rewrite (3.52) as

$$\begin{aligned} (V^*)^T R_d V &= \gamma_3 |v_1|^2 + \gamma_2 |v_2|^2 + \gamma_2 |v_3|^2 + \cdots + \gamma_3 |v_{M_z-1}|^2 + \gamma_1 v_2^* v_1 \\ &+ \gamma_1 v_1^* v_2 + \gamma_1 v_3^* v_2 + \gamma_1 v_2^* v_3 + \cdots + \gamma_1 v_{M_z-1}^* v_{M_z-2} + \gamma_1 v_{M_z-2}^* v_{M_z-1} \end{aligned} \quad (3.53)$$

After some rearrangement one obtains

$$\begin{aligned} (V^*)^T R_d V &= \gamma_1 |v_1 + v_2|^2 + \gamma_1 |v_2 + v_3|^2 + \gamma_1 |v_3 + v_4|^2 + \cdots + \gamma_1 |v_{M_z-2} + v_{M_z-1}|^2 + \\ &(\gamma_3 - \gamma_1)|v_1|^2 + (\gamma_2 - 2\gamma_1)|v_2|^2 + (\gamma_2 - 2\gamma_1)|v_3|^2 + \cdots + (\gamma_3 - \gamma_1)|v_{M_z-1}|^2 \end{aligned} \quad (3.54)$$

Since $\gamma_3 > \gamma_1$ and $\gamma_2 > 2\gamma_1$, all terms in (3.54) are non-negative and therefore R_d is positive-definite. G_d can be shown to be positive-definite in a similar fashion. In summary, we have proven that all the terms in (3.50) are non-negative or positive and therefore the discrete transmission model using a fourth-order compact difference scheme satisfies all passivity requirements. From a numerical integration point of view, it is extremely useful to be able to validate that the (semi-discrete) system of the state equations resulting from the numerical approximation of the spatial derivatives is passive. The reason for this is that passivity guarantees stability and thus a stable

numerical solution will always be achieved with a stable integration algorithm. From a model-order reduction point of view, it is essential that the passivity of the discrete model is verified before the development of a passive reduced-order model.

3.5 **Discrete Model of an MTL**

Extension of the aforementioned development of the TL model in section 3.3 to the case of a MTL is straightforward. For a MTL with M active conductors, an equation analogous to (3.38) may be written. Once again, each conductor is uniformly discretized into M_z segments, and the notation $I_i^{(n)}$, $V_i^{(n)}$ is used to denote the value of the current and voltage at position $i \cdot \Delta z$ on the n$^{\text{th}}$ conductor. The resulting discrete model may then be cast in the form

$$\underbrace{\begin{bmatrix} \tilde{R}_d + s\tilde{L}_d & \tilde{D}_V \\ \tilde{D}_I & \tilde{G}_d + s\tilde{C}_d \end{bmatrix}}_{\tilde{P}+s\tilde{Q}} \underbrace{\begin{bmatrix} \tilde{I}_0(s) \\ \tilde{I}_t(s) \\ \tilde{I}_{M_z}(s) \\ \tilde{V}_t(s) \end{bmatrix}}_{\tilde{X}_T} + \begin{bmatrix} -\tilde{V}_A \\ 0 \\ \vdots \\ 0 \\ \tilde{V}_B \\ 0 \\ \vdots \\ 0 \end{bmatrix} = 0 \qquad (3.55)$$

where

$$\tilde{R}_d + s\tilde{L}_d = \begin{bmatrix} 0 & 0 & 0 & & \cdots & & 0 \\ 0 & \tilde{a}_3 & \tilde{a}_1 & & & & \vdots \\ 0 & \tilde{a}_1 & \tilde{a}_2 & \ddots & & & \vdots \\ \vdots & & \ddots & \ddots & & & \\ \vdots & & & \ddots & \tilde{a}_2 & \tilde{a}_1 & 0 \\ & & & & \tilde{a}_1 & \tilde{a}_3 & 0 \\ 0 & \cdots & & & 0 & 0 & 0 \end{bmatrix} \tag{3.56}$$

$$\tilde{D}_V = \begin{bmatrix} U_M & & & & & \\ -U_M & U_M & & & & \\ & -U_M & & & & \\ & & & \ddots & \ddots & \\ & & & & & U_M \\ & & & & & -U_M \end{bmatrix} \tag{3.57}$$

$$\tilde{D}_I = \begin{bmatrix} -U_M & U_M & & & \\ & -U_M & U_M & & \\ & & & \ddots & \ddots \\ & & & & -U_M & U_M \end{bmatrix} \tag{3.58}$$

$$\tilde{G}_d + s\tilde{C}_d = \begin{bmatrix} \tilde{A}_4 & \tilde{A}_1 & & & \\ \tilde{A}_1 & \tilde{A}_2 & \ddots & & \\ & \ddots & \ddots & \ddots & \\ & & \ddots & \tilde{A}_2 & \tilde{A}_1 \\ & & & \tilde{A}_1 & \tilde{A}_4 \end{bmatrix} \tag{3.59}$$

Here U_M is the identity matrix of dimension M ,

$\tilde{a}_i = \alpha_i(R(j.\Delta z) + sL((j.\Delta z)).\Delta z \quad , \quad i = 1,2,3 \quad , \quad j =$ Column Block Number in (3.56)

$\tilde{A}_i = \alpha_i(G(j.\Delta z) + sC(j.\Delta z)).\Delta z \quad , \quad i = 1,2,4 \quad , \quad j =$ Column Block Number in (3.59)

R , L , G , and C are p.u.l resistance, inductance, conductance and capacitance matrices of the multi-conductor TL respectively; calculated at discrete nodes in the interior of the line, $j.\Delta z$. The state vector consists of the following vectors

$$\tilde{I}_0(s) = \begin{bmatrix} I_0^{(1)}(s) \\ I_0^{(2)}(s) \\ \vdots \\ I_0^{(M)}(s) \end{bmatrix}$$

$$\tilde{I}_t(s) = \begin{bmatrix} \begin{bmatrix} I_{1/2}^{(1)}(s) \\ \vdots \\ I_{1/2}^{(M)}(s) \end{bmatrix} \\ \vdots \\ \begin{bmatrix} I_{M_z-1/2}^{(1)}(s) \\ \vdots \\ I_{M_z-1/2}^{(M)}(s) \end{bmatrix} \end{bmatrix}$$

$$\tilde{I}_{M_z}(s) = \begin{bmatrix} I_{M_z}^{(1)}(s) \\ I_{M_z}^{(2)}(s) \\ \vdots \\ I_{M_z}^{(M)}(s) \end{bmatrix}$$

$$\tilde{V}_t(s) = \begin{bmatrix} \begin{bmatrix} V_0^{(1)}(s) \\ \vdots \\ V_0^{(M)}(s) \end{bmatrix} \\ \vdots \\ \begin{bmatrix} V_{M_z}^{(1)}(s) \\ \vdots \\ V_{M_z}^{(M)}(s) \end{bmatrix} \end{bmatrix}$$

$$\tilde{V}_A(s) = \begin{bmatrix} V_A^{(1)}(s) \\ \vdots \\ V_A^{(M)}(s) \end{bmatrix}$$

$$\tilde{V}_B(s) = \begin{bmatrix} V_B^{(1)}(s) \\ \vdots \\ V_B^{(M)}(s) \end{bmatrix}$$

In a manner similar to that for the case of the single line, a selection matrix, $\tilde{F}$, is introduced to map the transmission-line port voltages to the state vector, $\tilde{X}_T$

$$\begin{bmatrix} -\tilde{V}_A & 0 & \cdots & 0 & \tilde{V}_B & 0 & \cdots & 0 \end{bmatrix}^T = -\tilde{F} \begin{bmatrix} \tilde{V}_A \\ \tilde{V}_B \end{bmatrix} \tag{3.60}$$

and

$$\begin{bmatrix} \tilde{I}_A \\ \tilde{I}_B \end{bmatrix} = \tilde{F}^T \tilde{X}_T$$

where

$$\tilde{F} = \begin{bmatrix} U_M & 0 \\ 0 & 0 \\ \vdots & \vdots \\ 0 & 0 \\ -U_M & 0 \\ 0 & 0 \\ \vdots & \vdots \\ 0 & 0 \end{bmatrix}$$

Here $\tilde{I}_A$ and $\tilde{I}_B$ are current vectors at the near- and far-end terminals, respectively.

CHAPTER 4 NEW EFFICIENT AND PASSIVE FREQUENCY DEPENDENT MULTI-CONDUCTOR TRANSMISSION LINE MODEL

4.1 Introduction

Computer simulation of broadband digital pulses on high-speed interconnects that exhibits frequency dependent ohmic loss due to skin effect, requires the use of special transmission line models with per unit length resistance and inductance values that are functions of frequency. The extra modeling and simulation complexity introduced by this frequency dependence becomes necessary as clock frequencies in high performance systems are well surpassing the GHz boundary. Frequency dependant loss effects propagation delay, signal distortion, and high-frequency attenuation. While in the past such analysis was considered relevant to interconnects with cross-sectional dimensions in the order of many microns, it is now becoming an issue of concern even for conductors with dimensions as small as 1 μm. For example, effective bandwidth of a 1 GHz clock signal with rise and fall times less than 0.1 ns is about 10 GHz. Considering that for copper the skin depth at 10GHz is about 0.7 μm, it is apparent that skin effect must be accounted for in the calculation of the per-unit-length resistance of a wire of cross-sectional dimensions typical of re-distribution layers and even on-chip interconnections.

In the previous chapter, the application of compact differences to the spatial discretization was used to develop a computationally efficient discrete model for multi-conductor interconnects in such a manner that it was compatible with passive reduced order macromodeling algorithms. In this chapter, the same methodology is expanded for the development of a discrete model for interconnects with per-unit-length, frequency dependent resistance and inductance and with the assumption that dispersion due to the dielectric substrate is negligible. Initially, the frequency dependence of the off-diagonal resistance and impedance elements is ignored. In interconnects with weak coupling, such a model is sufficient and helps keep the number of unknowns in the discrete approximation small. Later, the model is expanded to take into account the frequency dependence of off-diagonal impedance elements as well.

For simplicity, the impedance and admittance parameters of the transmission lines are assumed to be position-independent. The extension of the model to interconnects with position-dependent parameters is possible. However, it is not in the scope of this work and will not be discussed here.

Again, one of the main objectives for the proposed model is that the resulting discrete form of Telegrapher's equations constitutes a passive system and is compatible with passive, reduced-order macromodeling algorithms, which will be discussed later in Chapter 5.

4.2 Discrete Model of Interconnects with Frequency Dependent Self Ohmic Loss

For clarity, the development of the proposed model is presented for the simple case of a two-conductor transmission line. Its extension to multiconductor transmission lines (MTLs) is straightforward once the state representation of the two-conductor system is in place.

The interconnect voltage and current satisfy the system of Telegrapher's equations stated in (3.1) and (3.2) with the exception that here p.u.l resistance, $R(s)$, and p.u.l inductance, $L(s)$, of the transmission line are assumed to be frequency dependent.

A discrete version of the system is obtained using compact differences for a spatial discretization that provides a high order of accuracy with a number of degrees of freedom much smaller than conventional models that use cascaded lumped RLC-circuit modeling of interconnects, specially for broadband (multi-GHz) discrete interconnect models. Assuming that the line is discretized into M_z segments of equal length Δz, the resulting system of state equations, written in a form suitable for multi-port macromodeling, is given by

$$\underbrace{\begin{bmatrix} 0 & 0 & 0 & \cdots & & 0 & 1 & & & & \\ 0 & d_3 & d_1 & & & \vdots & -1 & & & & \\ 0 & d_1 & d_2 & \ddots & & \vdots & & \ddots & \ddots & & \\ \vdots & & \ddots & \ddots & \ddots & & & & & & \\ \vdots & & & \ddots & d_2 & d_1 & 0 & & & & \\ & & & & d_1 & d_3 & 0 & & & & 1 \\ 0 & \cdots & & & 0 & 0 & 0 & & & & -1 \\ -1 & 1 & & & & & & g_4 & g_1 & & \\ & -1 & \ddots & & & & & g_1 & g_2 & \ddots & \\ & & \ddots & & & & & & \ddots & \ddots & \ddots \\ & & & & & & & & \ddots & g_2 & g_1 \\ & & & & & -1 & 1 & & & g_1 & g_4 \end{bmatrix}}_{G+sC}$$

$$\cdot \underbrace{\begin{bmatrix} I_0(s) \\ I_t(s) \\ I_{M_z}(s) \\ V_t(s) \end{bmatrix}}_{X} + \begin{bmatrix} -V_A \\ 0 \\ \vdots \\ 0 \\ V_B \\ 0 \\ \vdots \\ 0 \end{bmatrix} = 0 \qquad (4.1)$$

where V_A and V_B are the voltage values at the end points of the line (port voltage excitations), $I_t(s)$, $V_t(s)$ are the vectors of discrete current and voltage variables values at the interior of the line, respectively, while I_0 and I_{M_z} are the current variables at the end points of the line. The state matrix entries, d_i and g_i depend on the values of the p.u.l line parameters and grid size: $d_i = \alpha_i(R(s)+sL(s))\cdot\Delta z$ and $g_i = \alpha_i(G+sC)\cdot\Delta z$, where α_i is the appropriate compact difference coefficient discussed in section 3.3. Since the frequency dependence of the p.u.l. resistance and inductance is, in general, a complex, nonlinear function of s, the discrete model of

(4.1) is not appropriate for use in conjunction with model order reduction methods which are based on Krylov subspace iteration algorithms. To alleviate this problem, the results from the modal network theory of the skin effect in lossy conductors are utilized [3]. More specifically, it was shown in [3] that the frequency dependence of the current distribution inside a lossy conductor can be described in terms of an equivalent network of the type shown in Figure 4.1.

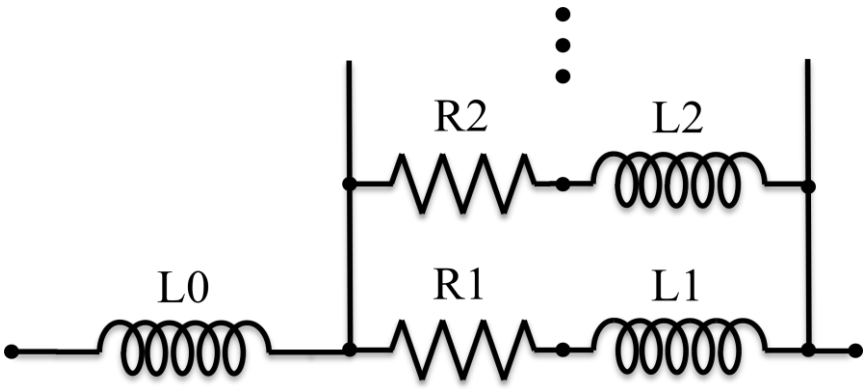

Figure 4.1 Modal network representation of a losssy conductor

As explained in [3] the network of Figure 4.1 is not merely a terminal equivalent circuit, but rather a complete network representation of the current distribution over the cross section of the conductor, with each of the branches R_i-L_i corresponding to each of the modes in the modal decomposition of the current density over the cross section. In addition, the external inductance, L_0, corresponds to the p.u.l. inductance of the line that is obtained under the assumption of perfect conductors.

In view of Figure 4.1, it is apparent that the p.u.l. frequency dependent impedance of the lossy interconnect, $Z(s) = R(s) + sL(s)$, may be cast in the form

$$Z(s) = R_0 + sL_0 + \sum_i \frac{k_i s}{s + p_i} \tag{4.2}$$

where R_0 is the dc p.u.l. resistance of the line and L_0 is its p.u.l. external inductance, i.e., the inductance value that the line would have if the conductors were perfect.

Let us assume next that a methodology exists for obtaining the values of k_i, and p_i in an approximate (truncated) form of (4.2) where only Q terms are included in the series. Such a methodology is discussed in the next section. Introducing the variables

$$I^{(i)} = \frac{s}{s + p_i} I_t \quad , \quad \hat{I}^{(i)} = \frac{k_i}{s} I^{(i)} \tag{4.3}$$

where $i = 1, 2, \ldots, q$, it is straightforward to show that the system of (4.1) may be cast in the form

$$(P_1 + sP_2)\hat{X} + f = 0 \tag{4.4}$$

where, assuming for simplicity and compactness of the mathematical expressions that $q = 2$,

$$\hat{X} = [I_t^T, V_t^T, I^{(1)^T}, \hat{I}^{(1)^T}, I^{(2)^T}, \hat{I}^{(2)^T}]^T \tag{4.5}$$

$$P_1 = \begin{bmatrix} R_0 a_z & D_V & k_1 a_z & 0 & k_2 a_z & 0 \\ D_I & G a_y & 0 & 0 & 0 & 0 \\ -k_1 a_z & 0 & k_1 a_z & k_1 a_z & 0 & 0 \\ 0 & 0 & -k_1 a_z & 0 & 0 & 0 \\ -k_2 a_z & 0 & 0 & 0 & k_2 a_z & k_2 a_z \\ 0 & 0 & 0 & 0 & -k_2 a_z & 0 \end{bmatrix} \tag{4.6}$$

$$P_2 = \begin{bmatrix} L_0 a_z & 0 & 0 & 0 & 0 & 0 \\ 0 & C a_y & 0 & 0 & 0 & 0 \\ 0 & 0 & 0 & 0 & 0 & 0 \\ 0 & 0 & 0 & \frac{k_1}{p_1} a_z & 0 & 0 \\ 0 & 0 & 0 & 0 & 0 & 0 \\ 0 & 0 & 0 & 0 & 0 & \frac{k_2}{p_2} a_z \end{bmatrix} \tag{4.7}$$

In the above matrices the following definitions have been used

$$a_z = \begin{bmatrix} a_3 & a_1 & 0 & \cdots & 0 & 0 \\ a_1 & a_2 & a_1 & \cdots & 0 & 0 \\ 0 & a_1 & a_2 & \cdots & 0 & 0 \\ \vdots & \vdots & \vdots & \ddots & \vdots & \vdots \\ 0 & 0 & 0 & \cdots & a_2 & a_1 \\ 0 & 0 & 0 & \cdots & a_1 & a_3 \end{bmatrix} \tag{4.8}$$

$$a_y = \begin{bmatrix} a_4 & a_1 & 0 & \cdots & 0 & 0 \\ a_1 & a_2 & a_1 & \cdots & 0 & 0 \\ 0 & a_1 & a_2 & \cdots & 0 & 0 \\ \vdots & \vdots & \vdots & \ddots & \vdots & \vdots \\ 0 & 0 & 0 & \cdots & a_2 & a_1 \\ 0 & 0 & 0 & \cdots & a_1 & a_4 \end{bmatrix} \tag{4.9}$$

$$D_V = \begin{bmatrix} 1 & \ddots & \\ -1 & \ddots & \\ & & 1 \\ & & -1 \end{bmatrix} \tag{4.10}$$

and $D_I = -D_V{}^T$. In the above it is assumed that $a_i = \alpha_i \Delta z$ where α_i are the appropriate compact difference coefficients that were discussed in section 3.3.

Under the assumption that k_i and p_i in (4.2) are positive, it is apparent from the above expressions that the matrices $P_1 + P_1^T$ and $P_2 + P_2{}^T$ are non-negative definite. Hence, as will be discussed in Chapter 5, it satisfies conditions to use PRIMA in order to generate a guaranteed-passive reduced-order model.

The extension of this approach to the case of a multiconductor system with N active conductors can be developed in a very similar fashion. In particular, the final form of the extended system of equations has the same form as that for the two-conductor case, except for the fact that the matrix elements in P_1 and P_2 now become block matrices in order to account for the M voltage and current vectors and the inductive and capacitive couplings between them.

The development of the pole/residue representation of (4.2) for the elements of the p.u.l. frequency dependent impedance matrix for the multiconductor transmission line (MTL) begins with the problem of calculating the p.u.l. resistance and inductance matrix at a specific frequency. The detail for the methodology for solving this problem is presented in Chapter 2.

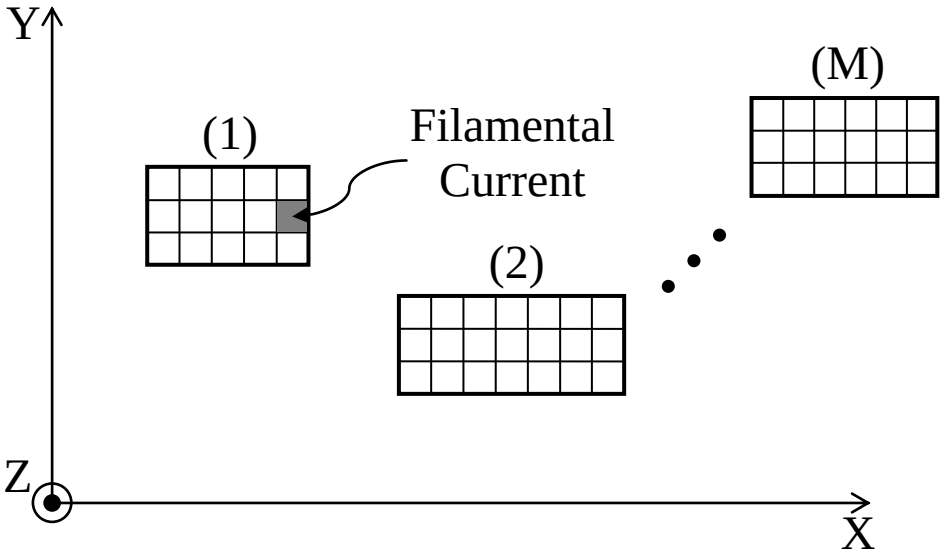

Figure 4.2 Discritization of conductor cross sections in an MTL for the purpose of frequency-dependent current distribution calculation.

Referring to the interconnect cross-sectional geometry of Figure 4.2, the conductor cross sections are discretized into rectangular elements of dimension smaller than the skin depth inside the conductor at the maximum frequency of interest. Such a discretization facilitates the discrete approximation of the (*z*-directed) current density over the cross section of each conductor. Essentially, the inhomogeneous current flow through the conductor has been approximated in terms of a set of filamentary current elements whose cross sections fill up the cross section of the conductor. Assuming that the discrete current density assumes a constant value over the area of each element, the following system of equations is derived for the filamentary currents,

$$\underbrace{\begin{bmatrix} \Delta V_1 \\ \Delta V_2 \\ \vdots \\ \Delta V_M \end{bmatrix}}_{\Delta V} = \underbrace{\begin{bmatrix} R_1 & & & \\ & R_2 & & \\ & & \ddots & \\ & & & R_M \end{bmatrix}}_{R} \begin{bmatrix} I_1 \\ I_2 \\ \vdots \\ I_M \end{bmatrix} + s \underbrace{\begin{bmatrix} L_{11} & L_{12} & \cdots & L_{1M} \\ L_{21} & L_{22} & \cdots & L_{2M} \\ \vdots & \vdots & \ddots & \vdots \\ L_{M1} & L_{M2} & \cdots & L_{MM} \end{bmatrix}}_{L} \begin{bmatrix} I_1 \\ I_2 \\ \vdots \\ I_M \end{bmatrix} \tag{4.11}$$

where the following definitions apply:

R_m is a diagonal matrix of size N_m containing the p.u.l. (dc) resistance of the filaments in the m^{th} conductor;

L_{mk} is a N_m by N_k matrix containing the p.u.l. partial inductances between the filaments in conductors m and k;

ΔV_m is a vector of size N_m containing the voltage drops p.u.l. along the filaments in the m^{th} conductor:

$$\Delta V_m = \begin{bmatrix} \Delta v_m & \Delta v_m & \cdots & \Delta v_m \end{bmatrix}^T \tag{4.12}$$

I_m is a vector of size N_m containing the filament currents in the m^{th} conductor;

M is the number of conductors;

N_m is the number of filaments in the m^{th} conductor.

We next introduce a selector matrix B such that

$$B = \begin{bmatrix} 1_1 & 0 & \cdots & 0 \\ 0 & 1_2 & \cdots & 0 \\ \vdots & \vdots & \ddots & \vdots \\ 0 & 0 & \cdots & 1_M \end{bmatrix} \tag{4.13}$$

where, $1_i = \begin{bmatrix} 1 & 1 & \cdots & 1 \end{bmatrix}^T$ is a vector of length N_i . Then defining I as the vector of conductor currents and ΔV as the vector p.u.l. voltage drops along the conductors, the p.u.l. impedance matrix, $Z(s)$, can be found from the solution of the system:

$$\begin{bmatrix} R+sL & -B \\ B^T & 0 \end{bmatrix} X = EI \qquad \Delta V = E^T X \tag{4.14}$$

or,

$$Z(s) = E^T \begin{bmatrix} R+sL & -B \\ B^T & 0 \end{bmatrix}^{-1} E \tag{4.15}$$

where $E = \begin{bmatrix} 0 & \cdots & 0 & U_M \end{bmatrix}^T$, U_M being an identity matrix of size M . It can be shown that $Z(s)$ is a passive transfer function [2] and its order is $N = \sum_{i=1}^{M} N_i$, which is generally very large for efficient waveform simulation. Therefore, it should be replaced with a reduced order, yet passive approximation, $\hat{Z}(s)$. For this purpose, since the circuit equations given in (4.14) are in the proper form for passive model order reduction, we would have used PRIMA. However, since PRIMA is a block order reduction technique, for an acceptable accuracy the order of the reduced system should be equal to a multiple of the number of conductors in the system.

There are two potential ways to alleviate this problem. The first solution is to increase the order of the reduced model. However, this method is not appealing since it compromises the efficiency of the numerical analysis of the overall system. This means that the order might still be unacceptable for efficient simulation.

An alternative technique is to break the system of equations for the MTL system into smaller blocks and apply model order reduction to each block one at a time. The later technique is more practical when field coupling between interconnects is not too strong. This methodology is used in this section since the frequency dependence of off-diagonal entries of $Z(s)$ is ignored here. For this purpose, PRIMA is applied to find each diagonal entry of the impedance matrix individually and off-diagonal elements are calculated analytically.

4.2.1 Approximation of the Diagonal Elements of $\hat{Z}(s)$

As stated above, there is a concern about the numerical accuracy or efficiency of the reduced order model that approximates the frequency dependent impedance of a system of multi-line transmission lines. Thus, in order to restrict the number of poles in the model to reasonably small values, a method is proposed here which finds the entries of $\hat{Z}(s)$ separately and still preserves the passivity.

Consider the diagonal element of $Z(s)$,

$$z_{jj}(s) = e_j^T \begin{bmatrix} R+sL & -B \\ B^T & 0 \end{bmatrix}^{-1} e_j \tag{4.16}$$

where e_j is the *j*-th column of E. In state equation form, this becomes

$$\begin{bmatrix} R+sL & -B \\ B^T & 0 \end{bmatrix}^{-1} X = e_j i_j \quad , \quad \Delta V_j = e_j^T X \tag{4.17}$$

The admittance quantity, $Y_j(s)$, is defined as

$$Y_j(s) = \frac{1}{z_{jj}} \tag{4.18}$$

The state equation form for $Y_j(s)$ can be derived from (4.17) and (4.18) as

$$\begin{bmatrix} \begin{bmatrix} R+sL & -B \\ B^T & 0 \end{bmatrix} & -e_j \\ e_j^T & 0 \end{bmatrix} \begin{bmatrix} X \\ i_j \end{bmatrix} = \begin{bmatrix} 0 \\ \vdots \\ 0 \\ 1 \end{bmatrix} \Delta V_j$$

$$i_j = \begin{bmatrix} 0 & \cdots & 0 & 1 \end{bmatrix} \begin{bmatrix} X \\ i_j \end{bmatrix} \tag{4.19}$$

PRIMA may now be used in conjunction with the above system to generate a Padé approximation, $\hat{Y}_j(s)$, for $Y_j(s)$. Since the above system corresponds to an RL circuit, $\hat{Y}_j(s)$ is a *q*-th order Padé approximation whose poles and zeros are all real negative numbers.

$$\hat{Y}_j(s) = \frac{b_0 + b_1 s + \cdots + b_{q-1} s^{q-1}}{1 + a_1 s + \cdots + a_q s^q} \tag{4.20}$$

Consequently, $\hat{z}_{jj}(s)$ can be found as

$$\hat{z}_{jj}(s) = \frac{1}{\hat{Y}_j(s)} = \frac{1 + a_1 s + \cdots + a_q s^q}{b_0 + b_1 s + \cdots + b_{q-1} s^{q-1}} \tag{4.21}$$

Using partial fraction expansion techniques, $\hat{z}_{jj}(s)$ may be cast in the form

$$\hat{z}_{jj}(s) = R_0 + sL_0 + \sum_{i=1}^{q} \frac{k_i s}{s + p_i} \tag{4.22}$$

Since the poles and zeros of $\hat{z}_{jj}(s)$ are all real negative numbers it can be shown that all of the parameters in the above representation of $\hat{z}_{jj}(s)$ are positive. Through numerical experimentations it is found that the choice $q = 3$ leads to an acceptable level of accuracy in simulations for typical on-chip interconnects.

In this method, a multipoint PRIMA with two expansion frequency points is used. Frequency expansion points are one at dc and another one at a reasonably high real frequency $s = s_0$. One of the moments is selected from the dc expansion, and the remaining two from the $s = s_0$ expansion. We usually select $s_0 = f_{\max}$, where $f_{\max}$ is the maximum frequency of interest. By applying the PRIMA method successively we approximate all the diagonal elements in $\hat{Z}$. Note that since the inversion at dc is trivial the whole process actually requires only one real matrix inversion at $s = s_0$. Details of model order reduction techniques and PRIMA in particular will be discussed in the next chapter.

4.2.2 **Approximation of Off-Diagonal Elements of** $\hat{Z}(s)$

In this section the frequency dependency of the off-diagonal elements of $\hat{Z}(s)$ is neglected. This is due to the fact that for many cases when the interconnect coupling is weak, the dominant contribution to skin-effect dispersion is caused by the frequency dependence of the self-inductance and the self-resistance of the conductors.

Thus, in addition to the fact that for those cases it has negligible impact on simulation accuracy, this approximation helps keep the number of unknown small in the circuit simulation. However, the proposed methodology will be expanded in the next section to include the frequency dependency of all of the elements of $\hat{Z}(s)$ for cases where they need to be taken into account.

The inductance matrix M_L is calculated as

$$M_L = \frac{Z(s_0)}{s_0} \tag{4.23}$$

where the matrix $Z(s_0)$ has already been calculated through (4.15), and the off-diagonal elements are obtained as

$$z_{ij}(s) = M_{L_{ij}} s \tag{4.24}$$

Where $M_{L_{ij}}$ is the *i*-th element of the *j*-th column of the matrix M_L.

This concludes the calculation of all of the impedance matrix entries in a proper format suitable for model order reduction techniques that are based on Krylov subspace iteration algorithms. However, in order to use PRIMA, it is required that $\hat{Z}(s)$ is non-negative definite. Let's look at the positive-definiteness of $\hat{Z}(s)$.

4.2.3 **Positive-Definiteness of** $\hat{Z}(s)$

From (4.22) and (4.23), the reduced p.u.l. impedance matrix has the form

$$\hat{Z}(s) = R_0 + sL_0 + R(s) \tag{4.25}$$

The diagonal matrix R_0 has as elements the dc per-unit-length resistance of the conductors and thus it is positive-definite. The full matrix L_0 is, essentially, the external p.u.l. inductance matrix, which would have been obtained from a two-dimensional interconnect parameter extractor assuming perfect conductors. Therefore, since it represents a passive network, it is positive-definite as well. The diagonal matrix $R(s)$ describes the frequency dependence of the field penetration inside each conductor. $R(s)$ is essentially a diagonal matrix whose entries are $\sum_{i=1}^{q} \frac{k_i s}{s + p_i}$, where k_i and p_i are positive numbers and represent poles and residues of the frequency dependence self impedance of the conductors.

Since all of the parameters in (4.22) are positive, the p.u.l. impedance matrix $\hat{Z}(s)$ is positive definite if and only if the matrix L_0 is positive definite. Note that L_0 is equivalent to the matrix M_L given in (4.23) (which is always positive definite), expect for the diagonal terms which are computed as defined in step 1. Therefore, the positive-definiteness of L_0 cannot be proven rigorously at this point; nevertheless, in all numerical experiments performed thus far the matrix was always found to be positive definite. Since the dimension of the matrix is small (equal to the number of conductors in the line), its positive-definiteness is cheap to test numerically.

The proposed method is computationally very efficient because it requires only on inversion, that of the real matrix in (4.15). In addition, it doesn't require any

nonlinear optimization to force the positive definiteness. Finally, it is observed that, contrary to alternative approaches in which the frequency-dependence of the self-inductance and resistance in each conductor is modeled in the absence of adjacent conductors, the presented method is such that the impact of the proximity effect is taken into account although its frequency dependency is ignored.

4.2.4 **Summary of the Overall Algorithm**

The overall algorithm for the development of the reduced-order macro model for a network of dispersive interconnects is summarized as follows:

1) For each MTL system the conductor cross sections are discretized into filaments, and the matrix R of p.u.l. filament resistances, and L of partial filament inductances are generated based on calculations in section 2.5. These matrixes are then used for the generation of the p.u.l. inductance matrix M_L through equations (4.15), (4.23) and the definition $s_0 = f_{\max}$, where $f_{\max}$ is the maximum frequency of interest.
2) For each MTL, PRIMA is used to generate the modal network representation for the p.u.l. self-impedances z_{ii} according to (4.22). This step completes the development of the equivalent p.u.l. impedance matrix $\hat{Z}(s)$ of (4.25) for each MTL system.
3) For each MTL an MNA stamp is constructed.
4) PRIMA is used to generate a reduced-order macro model for the multi-port resulting from the interconnection of all MTL systems and any other lumped linear parts.

5) Macromodels are combined with non-linear driver and receiver models in a SPICE environment for subsequent transient simulation.

4.3 Discrete Model of Interconnects with Frequency Dependent Self and Mutual Ohmic Loss

The need for developing an accurate model for a system of high speed interconnects that is efficient and compatible with passive model order reduction algorithms has been outlined in previous chapters. In the model proposed in previous section, in order to enhance computational efficiency of the system simulations, only diagonal entries of the transmission line impedance were frequency dependent. Although, such model is sufficient for many cases where coupling between interconnects is not very strong such as package or mother-board interconnects, it doesn't accurately represent on chip interconnects where shortage of real-estates enforces tight proximity of interconnects. This effect is intensifies as the frequency of operation increases and thus demands for more accurate frequency dependent models.

In this section, a discrete multi-interconnect transmission line model is developed that not only is efficient and compatible with the passive, reduced-order macromodeling algorithms, but also has full (diagonal and off-diagonal) frequency dependent impedance matrix.

Similar to the previous model, the development of the new model begins with the formulation of the magneto-quasistatic problem of calculating the p.u.l. resistance and inductance of the MTL at a given frequency. The methodology for solving this

problem is based on the discretization of the conductor cross sections into rectangular elements of dimension smaller than the skin depth corresponding to the maximum frequency of interest [11]. Such discretization facilitates the discrete approximation of the inhomogeneous current density over cross section of each conductor in terms of a set of filamentary currents with cross sections equal to those resulted from the conductor's cross-sectional discretization. With this discretization, the law of magnetic induction leads to the system of equations in (4.11) for the filamentary currents. Then the p.u.l. impedance matrix, $Z(s)$, can be found from (4.15)

$$Z(s) = E^T \begin{bmatrix} R + sL & -B \\ B^T & 0 \end{bmatrix}^{-1} E \tag{4.26}$$

where R and L are, respectively, resistance and inductance matrices of the filaments as defined in (4.11); B is a selector matrix as defined in (4.13) and $E = \begin{bmatrix} 0 & \cdots & 0 & U_M \end{bmatrix}^T$, U_M being an identity matrix of size M.

Generally $Z(s)$ is too large for efficient waveform simulation, therefore it should be replaced with a reduced yet passive approximation. For this purpose PRIMA is used which is a Padé approximation technique based on the Krylov subspace method. However, since the above system corresponds to an *RL* circuit, direct use of passive order reduction techniques from (4.26) generates complex poles and residues [12].Therefore, the system of state equations in (4.11) must be modified. Introducing new variable vectors, ΔV_g and sI and applying a frequency shift, s_c, the system of state equation in (4.11) can be expanded into

$$\underbrace{\begin{bmatrix} (s+s_c)G & -U & s_cU & 0 \\ U & L & 0 & -B \\ s_cU & 0 & s_csL & -s_cB \\ 0 & B^T & s_cB^T & 0 \end{bmatrix}}_{\tilde{G}+s\tilde{C}} \underbrace{\begin{bmatrix} \Delta V_g \\ sI \\ I \\ \Delta V \end{bmatrix}}_{\tilde{X}} = \tilde{E}\cdot(s+s_c)I_{in}$$

$$\Delta V = \tilde{E}^T\tilde{X} \tag{4.27}$$

where $G = R^{-1}$, U is the identity matrix, $\tilde{E} = \begin{bmatrix} 0 & E^T \end{bmatrix}^T$, and ΔV_g is the p.u.l. voltage drop vector across each resistor elements of filaments while ΔV .is the vector of the p.u.l. voltage drops along the conductors.

From (4.27), the p.u.l. impedance matrix that relates transmission line port voltages ΔV to I_{in} is given by

$$Z(s) = (s+s_c)H(s) \tag{4.28}$$

$$H(s) = \tilde{E}^T(\tilde{G}+s\tilde{C})^{-1}\tilde{E} \tag{4.29}$$

PRIMA may now be used in conjunction with the system of (4.27) to generate a q-th Padé approximation of $H(s)$

$$\hat{H}(s) = \sum_{i=1}^{q}\frac{R_i}{s-P_i} \tag{4.30}$$

The p.u.l. impedance matrix is obtained from (4.28) and (4.30) and assumes the form

$$\hat{Z}(s) = (s + s_c)\sum_{i=1}^{q} \frac{R_i}{s - P_i} \tag{4.31}$$

where the poles, P_i are all real negative numbers and residues, R_i are real positive definite matrices. For reasons that will be apparent later, the positive frequency shift s_c is chosen to be smaller than all of the poles, P_i . It helps to keep state matrices nicely structured and improves the convergence of the algorithm over the frequency range of interest.

From (4.31) it is apparent that dispersion of both self and mutual impedances has been incorporated in the elements of the p.u.l. impedance matrix.

4.3.1 **Development of the Discrete Model**

For clarity, the development of the model is presented for the simple case of a two-conductor transmission line with the assumption that dispersion due to substrate is negligible.

The interconnect voltages and currents satisfy the system of Telegrapher's equations, (3.1) and (3.2), in the Laplace domain. A discrete version of the system in (4.1) is obtained by discretizing the line into M_z segments of equal length Δz and applying fourth order compact difference operators to approximate the spatial derivatives in the Telegrapher's equations. The state matrix entries d_i, depend on the values of the p.u.l. line parameters and grid size: $d_i = \alpha_i \cdot Z(s) \cdot \Delta z$, where $Z(s) = R(s) + sL(s)$ and α_i is the appropriate compact difference coefficient discussed

in section3.3. Here, both self and mutual entries of the impedance matrix, $Z(s)$, are frequency dependent.

In order to make (4.1) in an appropriate form for passive, Krylov subspace-based order reduction algorithms, impedance matrix is approximated by its pole/residue representation in (4.31). Introducing new variable vectors

$$I^{(i)} = \frac{s+s_c}{s+p_i} I_t \quad , \quad \hat{I}^{(i)} = \frac{p_i - s_c}{s+p_i} I_t \tag{4.32}$$

where $i = 1, 2, \ldots, q$. It is straightforward to show that the system of (4.1) may be cast in the form

$$(P_1 + sP_2)\hat{X} + \hat{f} = 0 \tag{4.33}$$

where

$$P_1 = \begin{bmatrix} 0 & D_v & R_1 a_z & 0 & R_2 a_z & 0 & \cdots \\ D_I & G a_y & 0 & 0 & 0 & 0 & \cdots \\ -R_1 a_z & 0 & R_1 a_z & R_1 a_z & 0 & 0 & \cdots \\ 0 & 0 & -R_1 a_z & \dfrac{R_1 s_c}{p_1 - s_c} a_z & 0 & 0 & \cdots \\ -R_2 a_z & 0 & 0 & 0 & R_2 a_z & R_2 a_z & \cdots \\ 0 & 0 & 0 & 0 & -R_2 a_z & \dfrac{R_2 s_c}{p_1 - s_c} a_z & \cdots \\ \vdots & \vdots & \vdots & \vdots & \vdots & \vdots & \ddots \end{bmatrix} \tag{4.34}$$

$$P_2 = \begin{bmatrix} 0 & 0 & 0 & 0 & 0 & 0 & \cdots \\ 0 & Ca_y & 0 & 0 & 0 & 0 & \cdots \\ 0 & 0 & 0 & 0 & 0 & 0 & \cdots \\ 0 & 0 & 0 & \dfrac{R_1}{p_1 - s_c} a_z & 0 & 0 & \cdots \\ 0 & 0 & 0 & 0 & 0 & 0 & \cdots \\ 0 & 0 & 0 & 0 & 0 & \dfrac{R_2}{p_1 - s_c} a_z & \cdots \\ \vdots & \vdots & \vdots & \vdots & \vdots & \vdots & \ddots \end{bmatrix} \tag{4.35}$$

$$\hat{X}^T = \begin{bmatrix} I_t^T & V_t^T & I^{(1)^T} & \hat{I}^{(1)^T} & I^{(2)^T} & \hat{I}^{(2)^T} & \cdots & I^{(q)^T} & \hat{I}^{(q)^T} \end{bmatrix} \tag{4.36}$$

In the above matrices the following definitions have been used

$$a_z = \begin{bmatrix} a_3 & a_1 & 0 & \cdots & 0 & 0 \\ a_1 & a_2 & a_1 & \cdots & 0 & 0 \\ 0 & a_1 & a_2 & \cdots & 0 & 0 \\ \vdots & \vdots & \vdots & \ddots & \vdots & \vdots \\ 0 & 0 & 0 & \cdots & a_2 & a_1 \\ 0 & 0 & 0 & \cdots & a_1 & a_3 \end{bmatrix} \tag{4.37}$$

$$a_y = \begin{bmatrix} a_4 & a_1 & 0 & \cdots & 0 & 0 \\ a_1 & a_2 & a_1 & \cdots & 0 & 0 \\ 0 & a_1 & a_2 & \cdots & 0 & 0 \\ \vdots & \vdots & \vdots & \ddots & \vdots & \vdots \\ 0 & 0 & 0 & \cdots & a_2 & a_1 \\ 0 & 0 & 0 & \cdots & a_1 & a_4 \end{bmatrix} \tag{4.38}$$

$$D_V = -D_I^T = \begin{bmatrix} 1 & & \\ -1 & \ddots & \\ & \ddots & 1 \\ & & -1 \end{bmatrix} \tag{4.39}$$

$$\hat{f} = \begin{bmatrix} -V_A & 0 & \cdots & 0 & V_B & 0 & \cdots & 0 \end{bmatrix}^T \tag{4.40}$$

The coefficients a_i are related to the compact difference coefficient α_i in the following fashion: $a_i = \alpha_i \Delta z$. Under assumption that in (4.31), R_i is positive, $0 < s_c < p_i$, and p_i is positive, it is apparent from above expressions that P_2 is symmetric and the matrices $P_1 + P_1^T$ and P_2 are non-negative definite. Hence PRIMA can be used to generate a guaranteed passive reduced-order model.

The extension of this approach to the case of a multi-conductor system with M active conductors can be developed in a very similar fashion. In particular, the final form of the extended system of equations has the same form with that for the two-conductor case except for the fact that the matrix elements in P_1 and P_2 become now block matrices in order to account for the M voltage and current vectors and the inductive and capacitive coupling between them.

CHAPTER 5 MODEL ORDER REDUCTION TECHNIQUES

In Chapter 3 and Chapter 4 an efficient discrete model for high-speed interconnects with ohmic losses was presented. For typical high-speed interconnect systems, such as high-speed data busses, the distributed discrete electromagnetic model can easily reach to the order of tens of thousands of degrees of freedom. Despite significant advances in system simulator tools, the transient analysis for such systems is hindered by the large number of degrees of freedom involved in the distributed electromagnetic models. Therefore, the direct use of such models in Spice-like simulators for electrical performance assessment and design optimization is prohibitive for circuits with the complexity encountered in realistic integrated electronic systems. To circumvent this issue, the system is partitioned into subsystems in a way that the interactions between them occur only through common physical ports as depicted in Figure 5.1. As a result, each subsystem can be analyzed individually and model order reduction techniques can be applied to generate a macromodel representation of them that exhibits the same behavior at their ports. Then, the generated macromodels along with other linear or non-linear circuit elements are integrated in Spice-like simulators for frequency or time domain simulations.

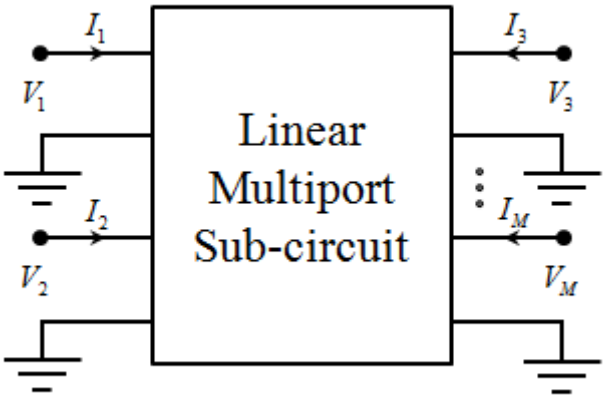

Figure 5.1 Processing of a linear sub-system into M port macromodel represented by its Y parameter matrix.

The generated reduced order macromodels are usually represented by their Z, Y, or S parameters in pole/residue format. Here the Y matrix representation is used although the same methodology can be applied for either type of system representation.

Let's start with the MNA standard system of state equations in (3.11a) and (3.11b):

$$(P+sQ)X(s)=FV_P(s) \tag{5.1}$$

$$I_P(s)=L^T X(s) \tag{5.2}$$

where matrices P, Q, $X(s)$, F, V_p, and I_p are defined in (3.15) through (3.19). The output selection matrix, L, is usually the same as F, but for the sake of generality is given a separate notation here.

$$A \equiv -P^{-1}Q \quad , \quad R \equiv P^{-1}F \tag{5.3}$$

Calculating the admittance matrix from (5.1) and (5.2), and using matrices defined in (5.3) we find that

$$Y(s) = L^T (U_n - sA)^{-1} R \tag{5.4}$$

where U_n is the identity matrix. Model reduction techniques finds the dominant poles of the admittance matrix and (5.4) indicates that poles of $Y(s)$ are in fact eigenvalues of A.

Three of the most popular model order reduction techniques will be discussed in this chapter, namely Asymptotic Waveform Evaluation (AWE) [13], the Arnoldi Algorithm [14], and Passive Reduced-order Interconnect Macromodeling Algorithm (PRIMA) [2]. Although the emphasis of this work is merely based on passive model order reductions such as PRIMA, the other two techniques are discussed for their relevant theoretical concepts.

5.1 **Asymptotic Waveform Evaluation (AWE)**

AWE is one of the original methods for model order reduction of a system which matches the first $2q$ moments of the actual and approximate Y-matrices in

order to obtain the q^{th} order Padé approximation. For simplicity let's assume the system has a single port. The extension to the multiport system will be straight forward.

Using the MacLaurin series expansion for $Y(s)$:

$$Y(s) = m_0 + m_1 s + m_2 s^2 + \cdots \tag{5.5}$$

where m_i, $i = 1, 2, \ldots$ are expansion moments and are calculated from (5.4) to be

$$m_i = L^T A^i R \tag{5.6}$$

Similarly, the MacLaurin series expansion for the approximated admittance, $\hat{Y}(s)$, is:

$$\hat{Y}(s) = \hat{m}_0 + \hat{m}_1 s + \hat{m}_2 s^2 + \cdots \tag{5.7}$$

where $\hat{m}_i$, $i = 1, 2, \ldots$ are the expansion moments. The q^{th} order Padé approximation of the admittance, $\hat{Y}(s)$, is formed by standard moment matching of the first q moments: $\hat{m}_i = m_i$ for $i = 1, 2, \ldots, 2q-1$. Next, $\hat{Y}(s)$ should be converted to the pole/residue format

$$\hat{Y}(s) = \frac{b_0 + b_1 s + \cdots + b_{q-1} s^{q-1}}{1 + a_1 s + \cdots + a_q s^q} \tag{5.8}$$

Here the objective is to find the b_i ($i = 0, 1, \ldots, q-1$) and a_i ($i = 1, 2, \ldots, q$) coefficients. From equating coefficients in (5.7) and (5.8):

$b_0 = m_0$

$b_1 = m_1 + m_0 a_1$

$$b_2 = m_2 + m_1 a_1 + m_0 a_2$$

$$\vdots$$

$$b_{q-1} = m_{q-1} + m_{q-2} a_1 + \cdots + m_0 a_{q-1}$$

$$0 = m_q + m_{q-1} a_1 + \cdots + m_0 a_q$$

$$0 = m_{q+1} + m_q a_1 + \cdots + m_1 a_q$$

$$\vdots$$

$$0 = m_{2q-1} + m_{2q-2} a_1 + \cdots + m_{q-1} a_q$$

Writing the above equations in matrix notation, we obtain:

$$\begin{bmatrix} 0 & 0 & \cdots & 0 \\ m_0 & 0 & \cdots & 0 \\ \vdots & \vdots & \ddots & \vdots \\ m_{q-2} & m_{q-3} & \cdots & m_0 \end{bmatrix} \begin{bmatrix} a_1 \\ a_2 \\ \vdots \\ a_{q-1} \end{bmatrix} + \begin{bmatrix} m_0 \\ m_1 \\ \vdots \\ m_{q-1} \end{bmatrix} = \begin{bmatrix} b_0 \\ b_1 \\ \vdots \\ b_{q-1} \end{bmatrix} \tag{5.9}$$

$$\begin{bmatrix} m_{q-1} & m_{q-2} & \cdots & m_0 \\ m_q & m_{q-1} & \cdots & m_1 \\ \vdots & \vdots & \ddots & \vdots \\ m_{2q-2} & m_{2q-3} & \cdots & m_{q-1} \end{bmatrix} \begin{bmatrix} a_1 \\ a_2 \\ \vdots \\ a_q \end{bmatrix} = - \begin{bmatrix} m_q \\ m_{q+1} \\ \vdots \\ m_{2q-1} \end{bmatrix} \tag{5.10}$$

To find the a_i ($i = 1, 2, \ldots, q$) coefficients, the Hankel matrix in (5.10) should be inverted. However, it tends to become an ill-conditioned matrix when the order increases beyond some value. Also, for broadband cases, AWE with multiple expansion points is needed [15], [16], and [17].

5.2 Passive Reduced-order Interconnect Macromodeling Algorithm (PRIMA)

As was discussed in Chapter 3 the passivity of the reduced order macromodel is essential in order to guarantee the stability of the whole system. Although stability of each individual macromodel can be enforced by eliminating the unstable poles, the stability of the overall system once the individual macromodels are connected is not guaranteed. However, due to the fact that integration of passive subsystems generates an overall passive system, which is by definition stable as well, this problem can be avoided if each macromodel is passive. For this purpose PRIMA is used to generate guaranteed passive reduced order macromodels.

PRIMA uses the Block Arnoldi algorithm [18] along with a congruence transformation to generate a guaranteed passive macromodel. The Block Arnoldi algorithm is Krylov space based and is known to be computationally more efficient and numerically more stable than AWE.

The PRIMA algorithm reduces the system matrix A in (5.3) to a small $q \times q$ block upper Hesenberg[1] matrix H_q such that

$$AV = VH_q \tag{5.11}$$

subject to

[1] A matrix is an upper Hessenberg if its *ij*-th element is zero when $i > j+1$

$$V^T V = U_q \tag{5.12}$$

where V is an $n \times q$ matrix consist of orthonormal columns spanning a properly constructed Krylov space, and U_q is identity matrix of dimension q. Columns of V are recursively filled to form an orthonormal basis for the Krylov subspace $Kr(A, R, k)$ which is defined as

$$Kr(A, R, k) = colsp\left[R, AR, A^2R, \ldots, A^k R \right] \tag{5.13}$$

where k is the nearest integer greater than q/n_p and n_p is number of ports. Equation (5.13) is a column space formed by R, AR, A^2R, …, $A^k R$. From (5.6), it is apparent that those matrices are in fact successive moments of the system, however, with improved condition due to the othonormality of the bases.

The change of variables, $X = V\hat{X}$, constrains the original state vector X of length n to the q dimensional subspace spanned by the columns of matrix V. Applying this change of variables to (5.1) and (5.2), and using matrix definitions in (5.3) leads to

$$\begin{aligned} (U_n - sA)V\hat{X} &= RV_P \\ I_P &= L^T V\hat{X} \end{aligned} \tag{5.14}$$

where U_n is identity matrix of dimension $n \times n$. In the block Arnoldi algorithm, (5.14) is combined with (5.11) and (5.12) to obtain

$$\hat{Y}(s) = L^T V (U_q - sH_q)^{-1} V^T R \tag{5.15}$$

where U_q is a $q \times q$ identity matrix.

The difference between the PRIMA algorithm as compared to the Arnoldi algorithm is that the aforementioned change of variables is directly applied to (5.1) and (5.2) to generate a new set of system matrices with orders much smaller than the original matrices. Consequently, passivity of the reduced system can be proven mathematically [2]. Using the change of variables, $X = V\hat{X}$, called a Congruence transformation [19], in (5.1) and (5.2) result in

$$(P + sQ)V\hat{X}(s) = FV_P(s) \tag{5.16}$$

$$I_P(s) = L^T V\hat{X}(s) \tag{5.17}$$

Multiplying both sides of (5.16) by V^T and regrouping the terms yields

$$\left((V^T PV) + s(V^T QV)\right)\hat{X}(s) = (V^T F)V_p(s) \tag{5.18}$$

$$I_P(s) = (V^T L)^T \hat{X}(s) \tag{5.19}$$

Therefore, the new reduced order system matrices are

$$\begin{aligned} \hat{P} &= V^T PV \\ \hat{Q} &= V^T QV \\ \hat{F} &= V^T F \\ \hat{L} &= V^T L \end{aligned} \tag{5.20}$$

Now the reduced admittance, $\hat{Y}(s)$, can be calculated from (5.18), (5.19), and (5.20) as

$$\hat{Y}(s) = \hat{L}^T (\hat{P} + s\hat{Q})^{-1} \hat{F} \tag{5.21}$$

Since the new system matrices are much smaller than the original ones, poles and zeros of $\hat{Y}(s)$ now can be easily computed from (5.21).

CHAPTER 6 NUMERICAL ANALYSIS

Examples in this chapter are meant to demonstrate the accuracy of the proposed MTL models as well as their use in conjunction with PRIMA for MTL model order reduction.

6.1 Efficient Passive Interconnect Model (UA-EPIM) for a Single TL

The first example involves the efficient passive modeling for single (not-coupled) transmission lines. The circuit shown in Figure 6.1 was analyzed using the model developed in Chapter 3 for interconnect systems whose their ohmic loss parameters are almost independent of frequency due to their physical dimensions or frequency of operation. For the purposes of transient simulation, an effective bandwidth of 15 GHz was assumed. Such a bandwidth is characteristic of a trapezoidal pulse with rise/fall times of about 20 ps. For this simulation a trapezoidal pulse of amplitude 5 V, width 250 ps, and rise and fall times of 25 ps was used. The resolution used in the discrete model was ~8 points per minimum wavelength. Once, the discrete model was developed, the PRIMA algorithm was used to generate a reduced-order model of order 90. Figure 6.2 compares the "exact" waveform, V_{out}, obtained through a SPICE simulation, with that produced by the generated

macromodel. Excellent agreement is observed, both in waveform shape and in the simulation of the propagation delay.

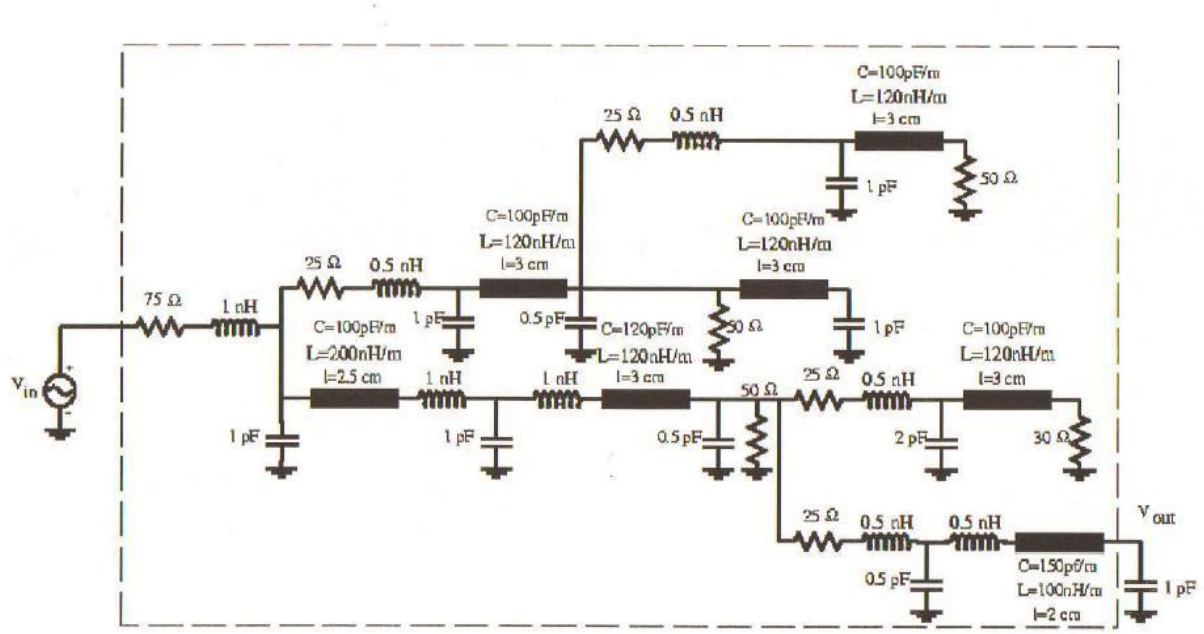

Figure 6.1 The circuit inside the dashed-line is represented by a 2-port Y-parameter marcromodel. Interconnects are modeled using fourth-order compact difference operators.

Figure 6.3 and Figure 6.4 depict the magnitude and phase, respectively, of the admittance parameter Y_{11} over the frequency bandwidth of interest. Notice that the agreement of the reduced order model (curve "UA-EPIM") with the discrete model (curve "UA-EPIM (no PRIMA)") is excellent over the entire frequency band. However, their agreement with the responses obtained through SPICE simulations using the exact transmission line model remains good only up to about 10 GHz.

Nevertheless, this accuracy was sufficient for the transient simulation, as Figure 6.2 clearly illustrates. Furthermore, the accuracy of the discrete model can be improved by increasing the number of nodes per minimum wavelength in the discretization of the voltage and current distributions along the transmission line.

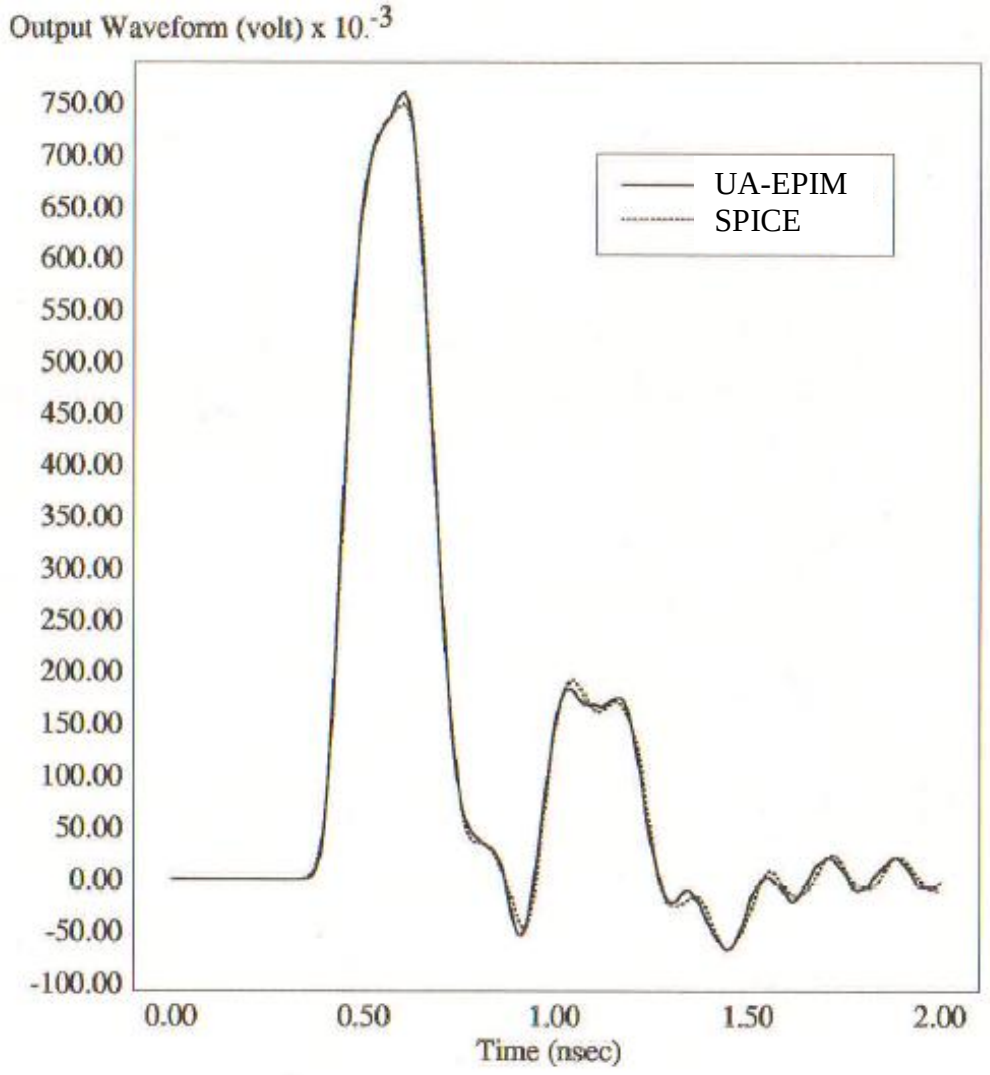

Figure 6.2 Comparison of the simulated output voltage waveform V_{out} for the interconnect circuit in Figure 6.1.

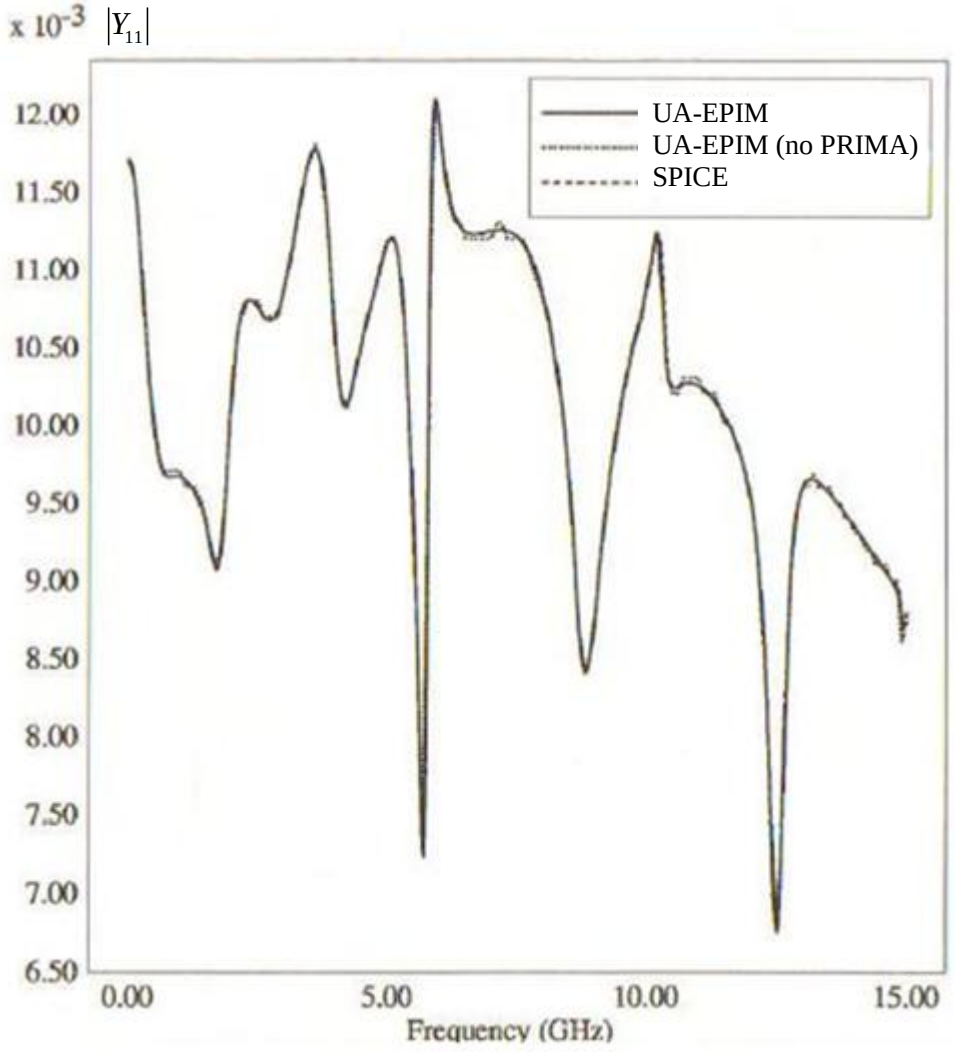

Figure 6.3 The magnitude of the frequency response of Y_{11} for the interconnect circuit in Figure 6.1.

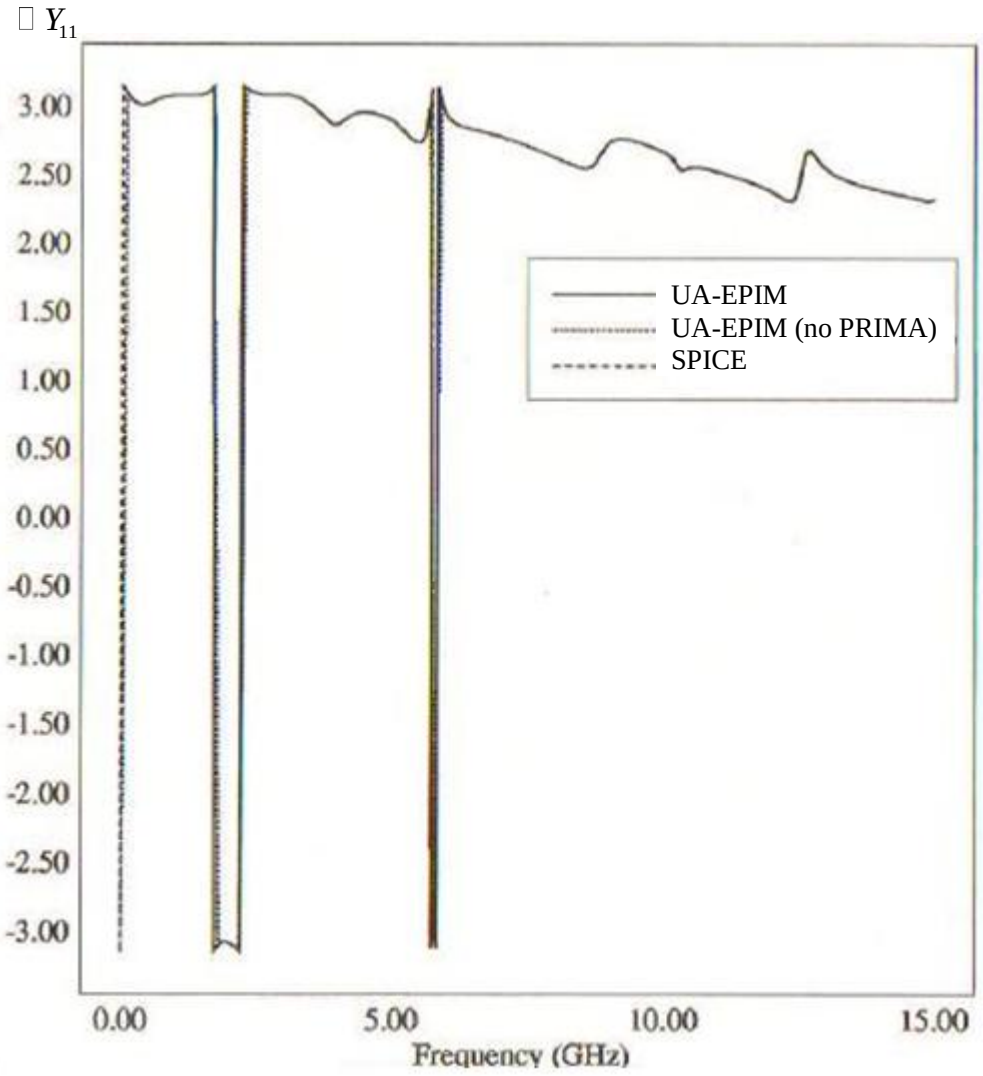

Figure 6.4 The phase of the frequency response of Y_{11} for the interconnect circuit in Figure 6.1.

6.2 Efficient Passive Interconnect Model (UA-EPIM) for MTL

This example considers the interconnect network depicted in Figure 6.5 which could represent the thin-film wiring of an on-package multi-line interconnection system. The interconnects are 3 cm long and have p.u.l. matrices of

$$L = \begin{bmatrix} 3.0564 & 0.9865 & 0.42008 \\ 0.9865 & 2.9678 & 0.9865 \\ 0.42008 & 0.9865 & 3.0564 \end{bmatrix} \quad nH/cm$$

$$C = \begin{bmatrix} 0.90112 & -0.16643 & -0.0111 \\ -0.16643 & 0.96521 & -0.16643 \\ -0.0111 & -0.16643 & 0.90112 \end{bmatrix} \quad pF/cm$$

$$R = \begin{bmatrix} 11.25 & 0 & 0 \\ 0 & 11.25 & 0 \\ 0 & 0 & 11.25 \end{bmatrix} \quad \Omega/cm$$

$$G = 0$$

The cross-sectional dimensions of the interconnections were selected such that the characteristic impedance of the individual lines (neglecting ohmic loss) is about 55 ohm. Dielectric loss is assumed negligible.

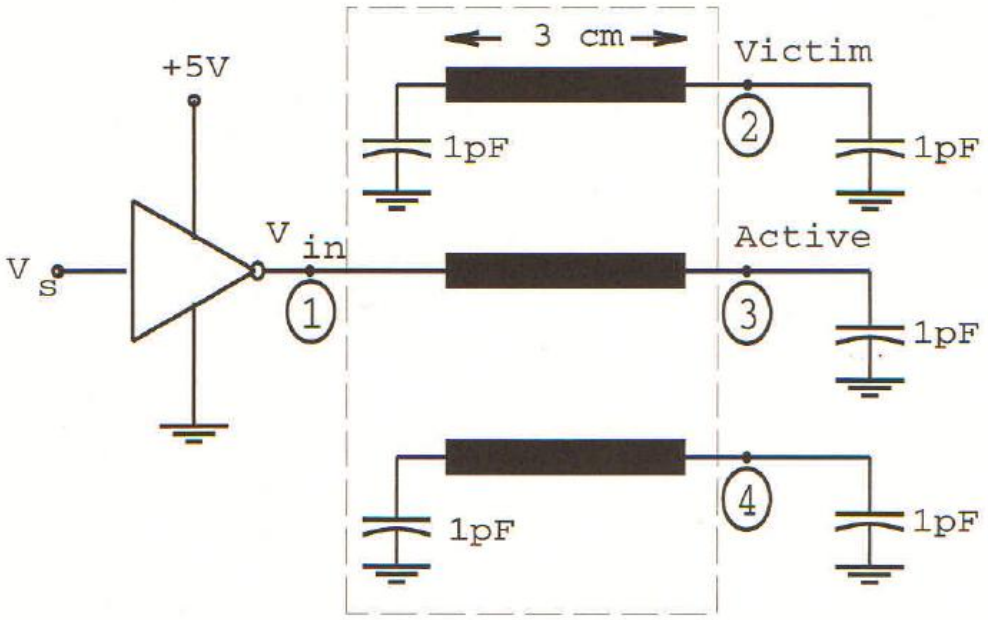

Figure 6.5 A circuit representing an on-chip interconnect system. The circuit inside the dashed line is represented by a 4-port *Y*-parameter macromodel.

The compact-difference discretization scheme proposed in Chapter 3 was used to generate a discrete model appropriate for simulation over a frequency bandwidth of at least 10 GHz. From the above p.u.l. parameters, approximate values for the phase velocities of the three fundamental modes of wave propagation on the MTL can be obtained. In this calculation, the p.u.l. resistance of the lines is neglected in order to avoid the issue of the frequency dependence of the phase velocity. A straight forward eigenvalue analysis of the matrix LC yields the phase velocities $v_{ph}^{(1)} = 17.68$ cm/ns, $v_{ph}^{(2)} = 20.39$ cm/ns, and $v_{ph}^{(3)} = 21.81$ cm/ns. For the 10 GHz bandwidth of interest, the minimum wavelength that must be resolved accurately is therefore, $\lambda_{\min} = v_{ph}^{(1)} / f_{\max} = 1.768$ cm. Consequently, at the maximum frequency of

interest the length of the line is approximately two wavelengths. For such an electrical size, use of the segmentation approach would require the discretization of the MTL into 40 segments for accurate transient waveform simulation. On the other hand, with the use of compact differences the number of segments is reduced to 16. For accurate simulation, the total number of variables prior to using PRIMA was 115 when using compact differences compared to 265 when using the segmentation approach.

PRIMA was used to generate a reduced-order macromodel for the four- port indicated by the dashed box in Figure 6.5. The order of the macromodel is 50. The magnitude of Y_{11}, calculated using the proposed compact difference model without model reduction (labeled as UA-EPIM(no PRIMA)), is compared to the one generated by the reduced-order model (labeled as UA-EPIM) in Figure 6.6. Also, shown in the same figure is the magnitude of Y_{11} obtained using an exponentially-accurate Chebyshev (pseudo-spectral) model of [20] (labeled as SPICE). Excellent agreement is observed.

The far-end waveforms for both the active and victim lines, for the case of a trapezoidal pulse excitation of amplitude 5 V, width 2.9 ns and rise and fall times of 100 ps, are shown in Figure 6.7. Clearly, they are in excellent agreement (the lines overlap each other) with those generated using the model of [20].

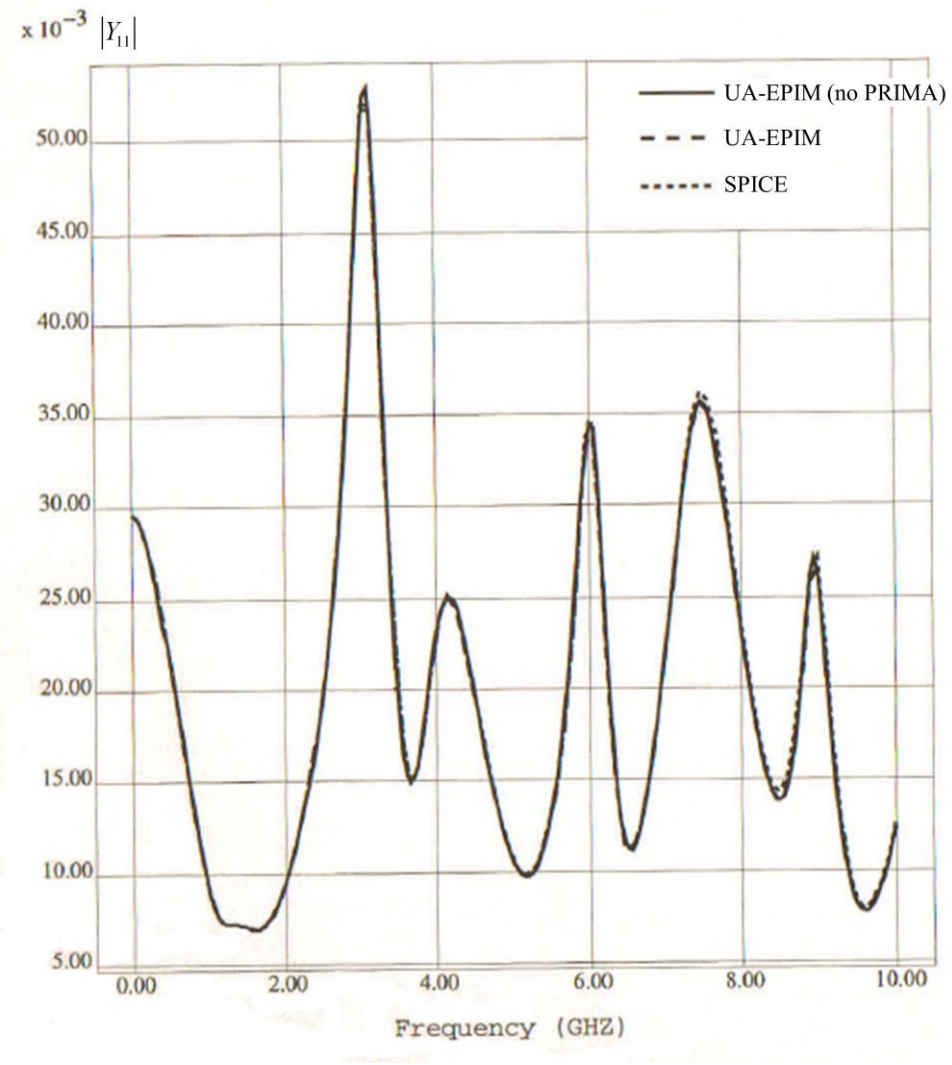

Figure 6.6 The magnitude of the frequency response of Y_{11} for the circuit of Figure 6.5.

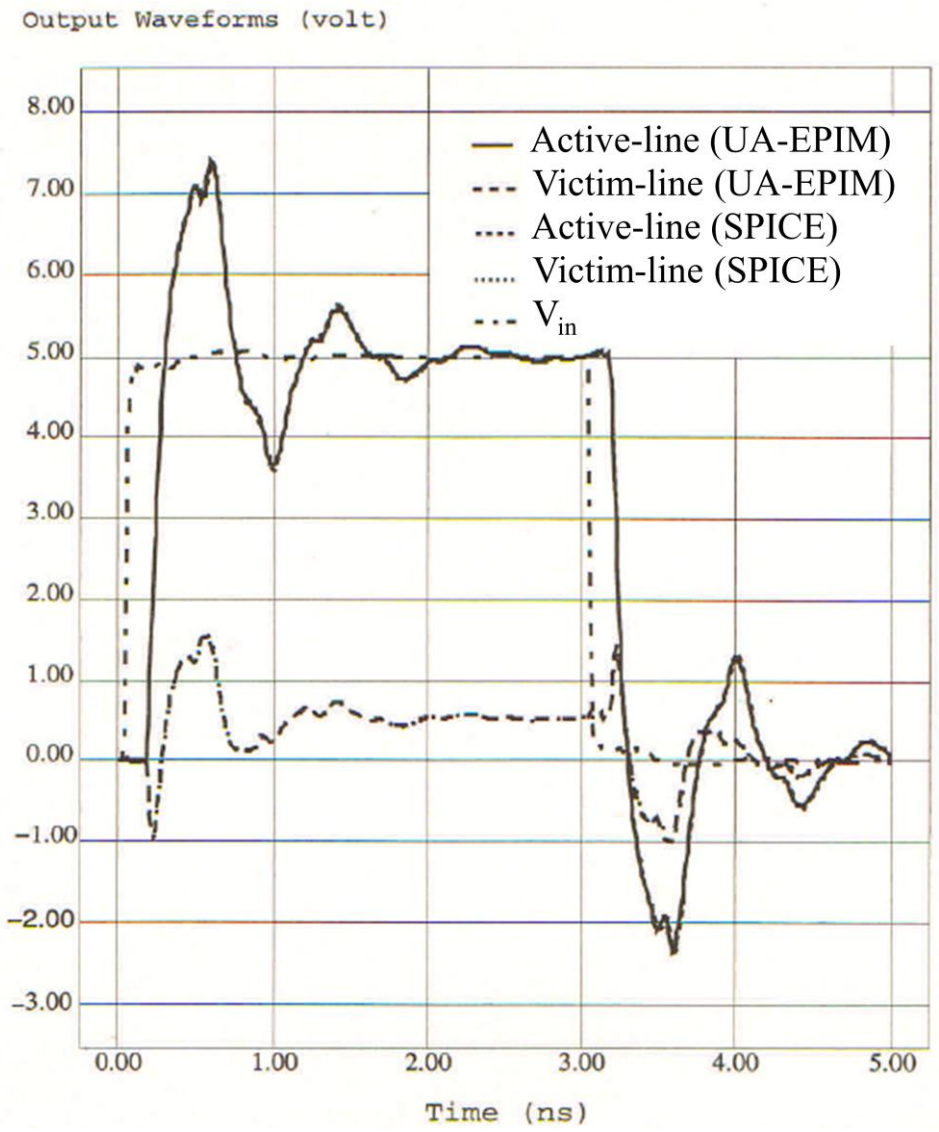

Figure 6.7 The simulated output voltage waveforms for the interconnection circuit in Figure 6.5.

6.3 Dispersive Efficient Passive Interconnect Model (UA-DEPIM1) for the Case of Frequency Dependent Self Ohmic Loss

The interconnect circuit from the previous section (Figure 6.5) is now analyzed using the methodology described in section 4.2, which takes into account the frequency dependence of ohmic loss for the self-impedance parameters. Since the dispersion due to the dielectric substrate is assumed negligible, only the p.u.l. inductance and resistance matrices exhibit frequency dependence. The copper conductors have rectangular cross sections of width 10 μm and thickness of 5 μm. They are placed 8.05 μm above ground, and the distance between them is 10 μm. The relative dielectric constant of the insulating substrate is taken to be $\varepsilon_r = 4$. The conductivity of the conductors is assumed to be 5.813×10^7 S/m.

Figure 6.8 and Figure 6.9 compare the real and imaginary parts of the general pole/residue representation of the p.u.l. frequency-dependent impedance matrix element z_{11} with the values calculated directly from [3]. The expansion frequency was selected to be $s_0 = 10$ GHz. The agreement is very good. Figure 6.10 depicts the magnitude of the admittance matrix element Y_{11} for the reduced model of the multiport macromodel indicated with the dashed rectangle in Figure 6.5. The order of the reduced model was 55. Again, very good agreement is observed between the PRIMA generated reduced-order model response for the multiport and the response obtained from the numerical model without order reduction.

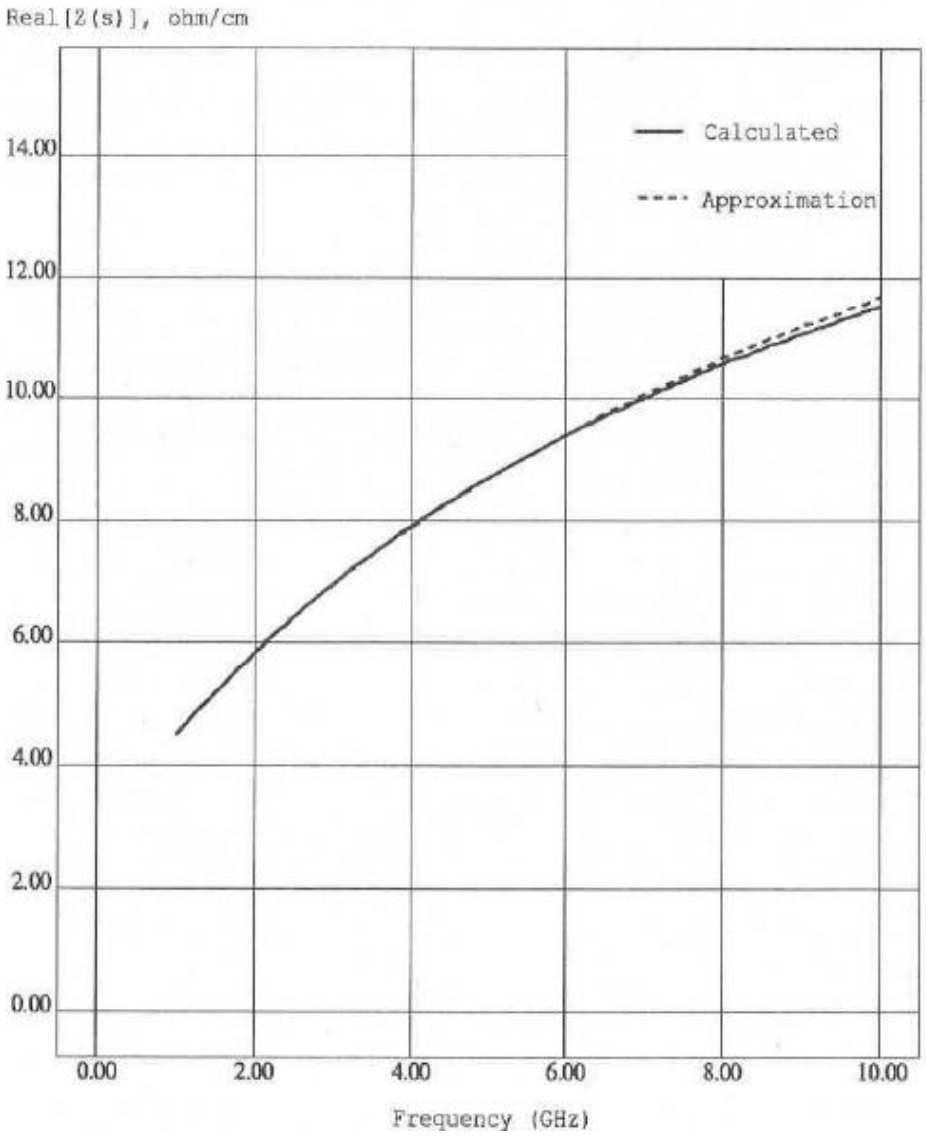

Figure 6.8 Comparison of the Padé approximation for the real part of the p.u.l. impedance z_{11} with the calculated value, obtained numerically from (4.16).

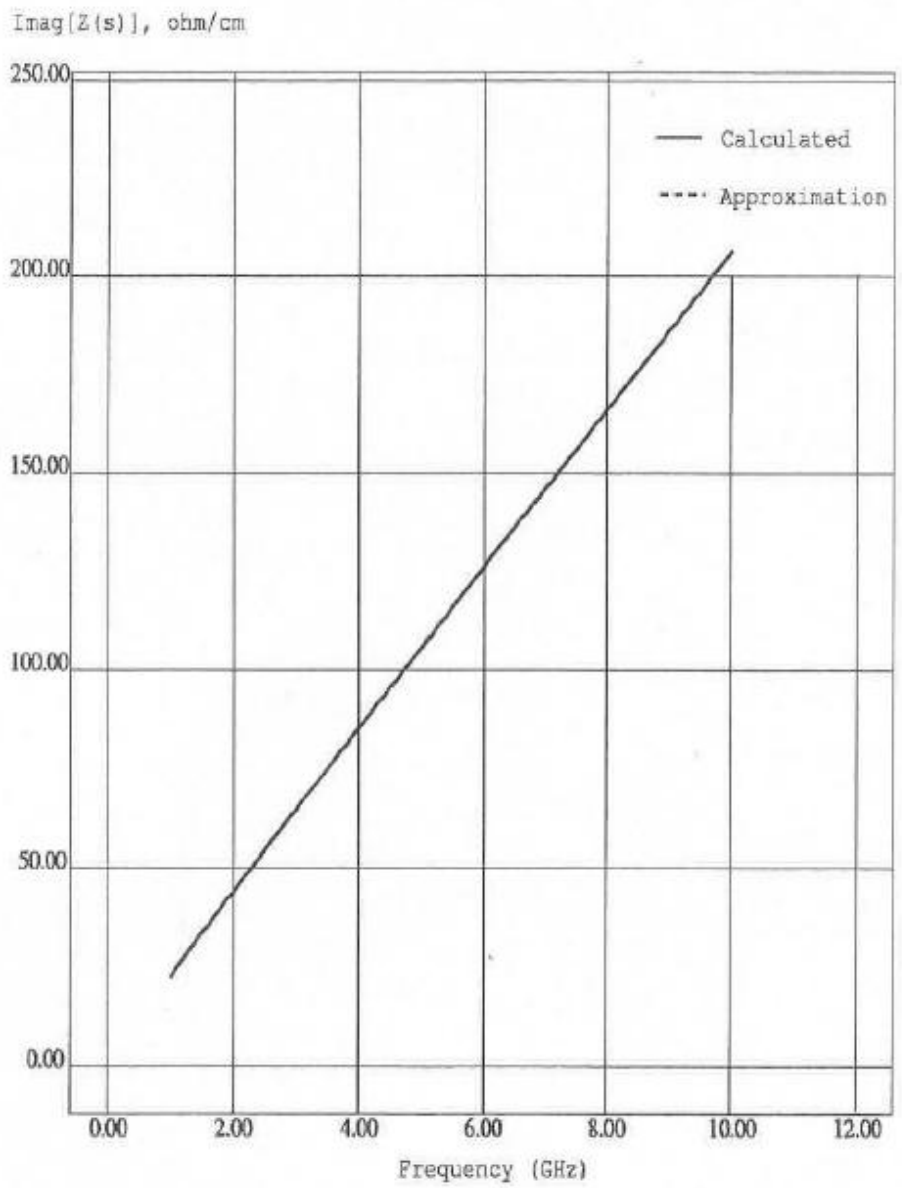

Figure 6.9 Comparison of the Padé approximation for the imaginary part of the p.u.l. impedance z_{11} with the calculated value, obtained numerically from (4.16).

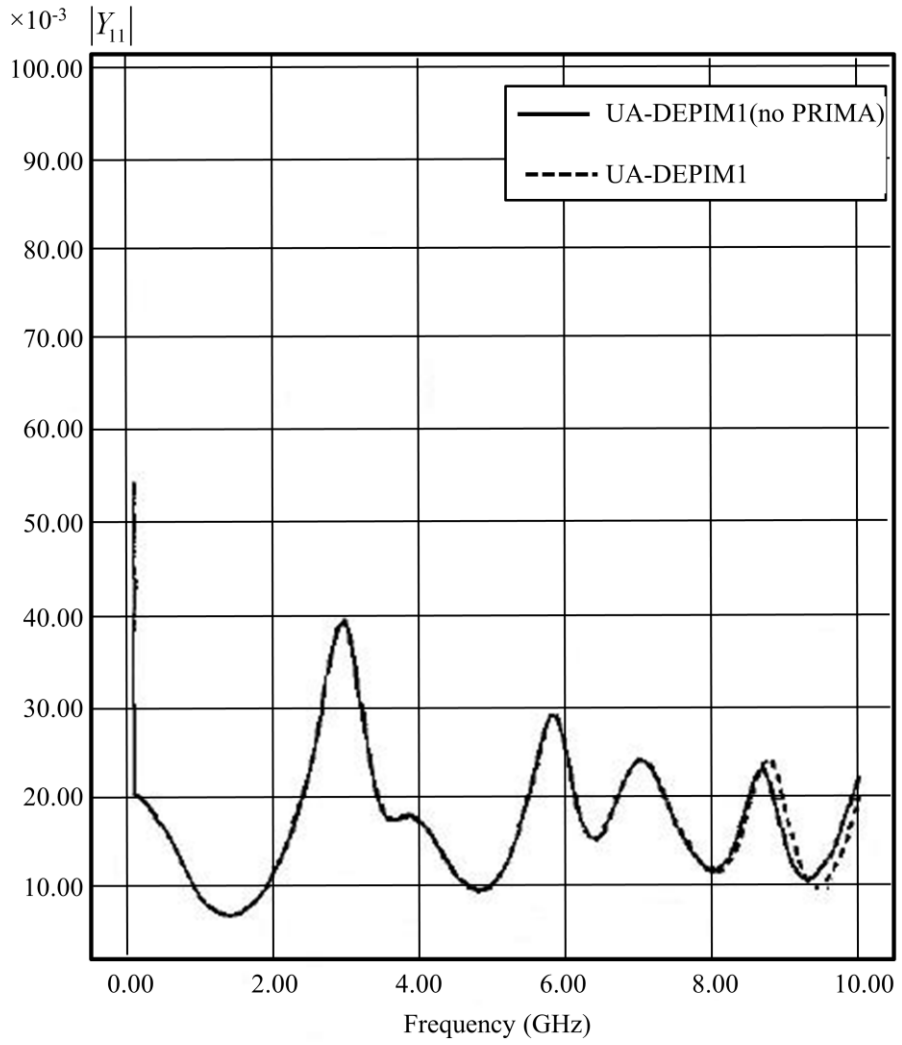

Figure 6.10 Magnitude of Y_{11} for the multiport interconnect of Figure 6.5.

Finally, Figure 6.11 and Figure 6.12 depict the calculated response at the outputs of the active and quiet lines, respectively. In particular, a comparison is provided between the waveforms obtained with and without taking into accounts the frequency dependence of the p.u.l. self-impedance values. The influence of frequency-dependent losses is apparent.

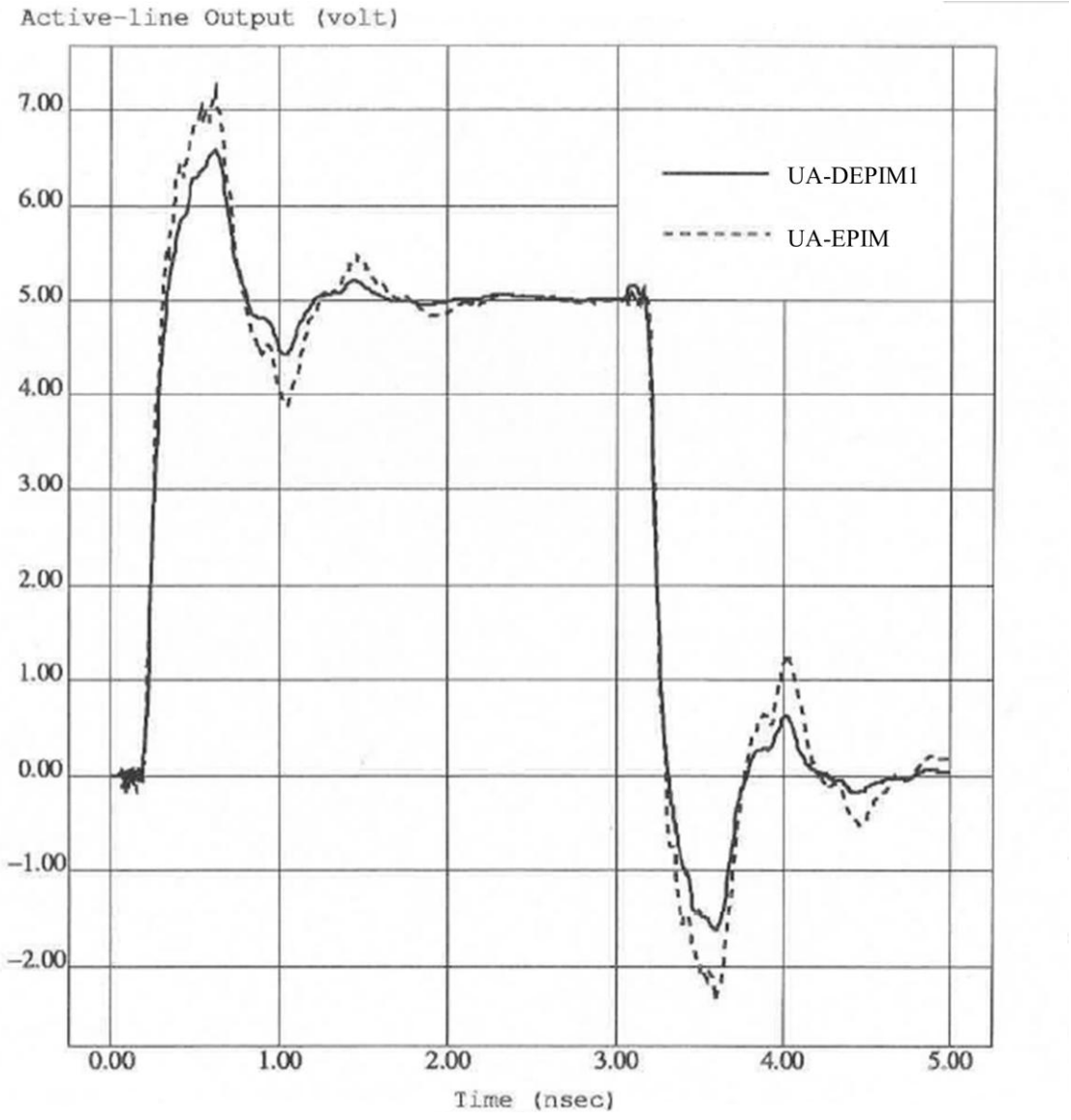

Figure 6.11 Calculated waveform at the output of the active line of the interconnect circuit in Figure 6.5. Solid line is for the case of frequency-dependent impedance while dashed line is for frequency independent impedance.

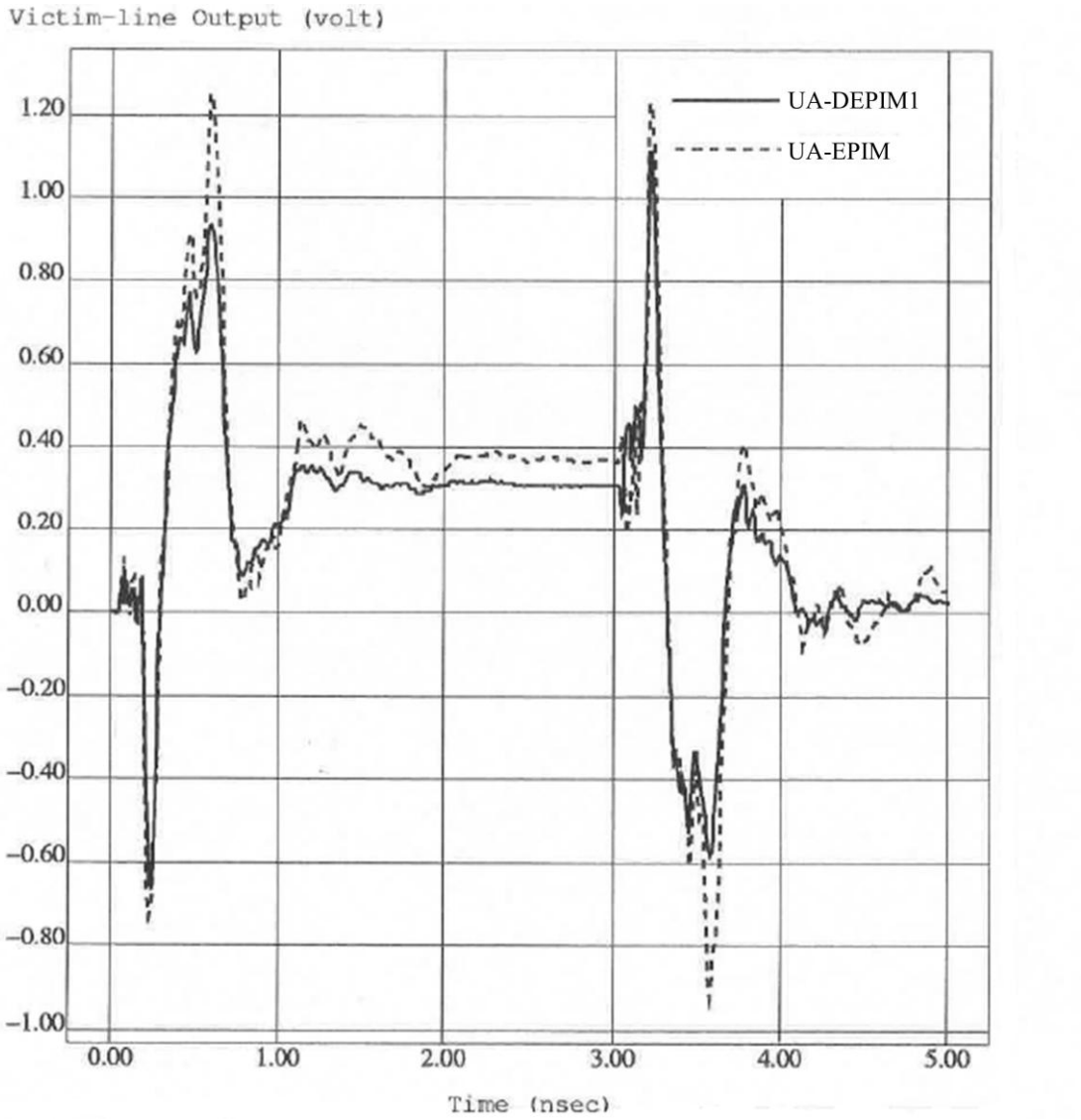

Figure 6.12 Calculated waveform at the output of the quiet line of the interconnect circuit in Figure 6.5. Solid line is for the case of frequency-dependent impedance while dashed line is for frequency independent impedance.

There is significant attenuation in the high-frequency part of the spectrum of the transient waveforms due to the skin effect which is not modeled using simply the dc value of the p.u.l. impedance.

6.4 Dispersive Efficient Passive Interconnect Model (UA-DEPIM2) for the Case of Frequency Dependent Self and Mutual Ohmic Loss

The coupled interconnect structure shown in Figure 6.13 was analyzed using the methodology discussed in section 4.3 which takes into account frequency dependence of both self and mutual ohmic losses. Since the dispersion due to the substrate is assumed negligible, only the p.u.l. inductance and resistance matrices exhibit frequency dependence. The interconnects are taken to be copper micro-strip lines which are 20 μm wide and 5 μm thick. They are placed 15 μm above the ground plane and 10 μm apart. The relative dielectric constant of the insulating substrate is taken to be $\varepsilon_r = 4$. The effective bandwidth of interest was considered to be 10 GHz.

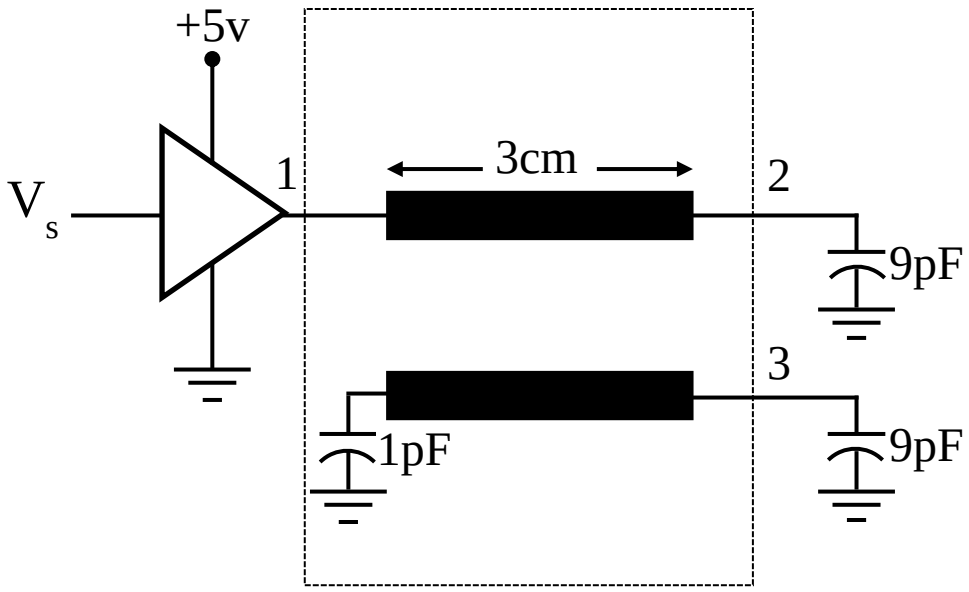

Figure 6.13 The high-speed digital interconnect circuit used in the simulations.

Figure 6.14 and Figure 6.15, respectively, compare the real and imaginary parts of the generated pole/residue representation of the p.u.l. frequency-dependent impedance matrix element z_{11} with the value calculated directly from (4.26). The expansion frequency was selected to be $s_0 = 10$ GHz. The agreement is very good.

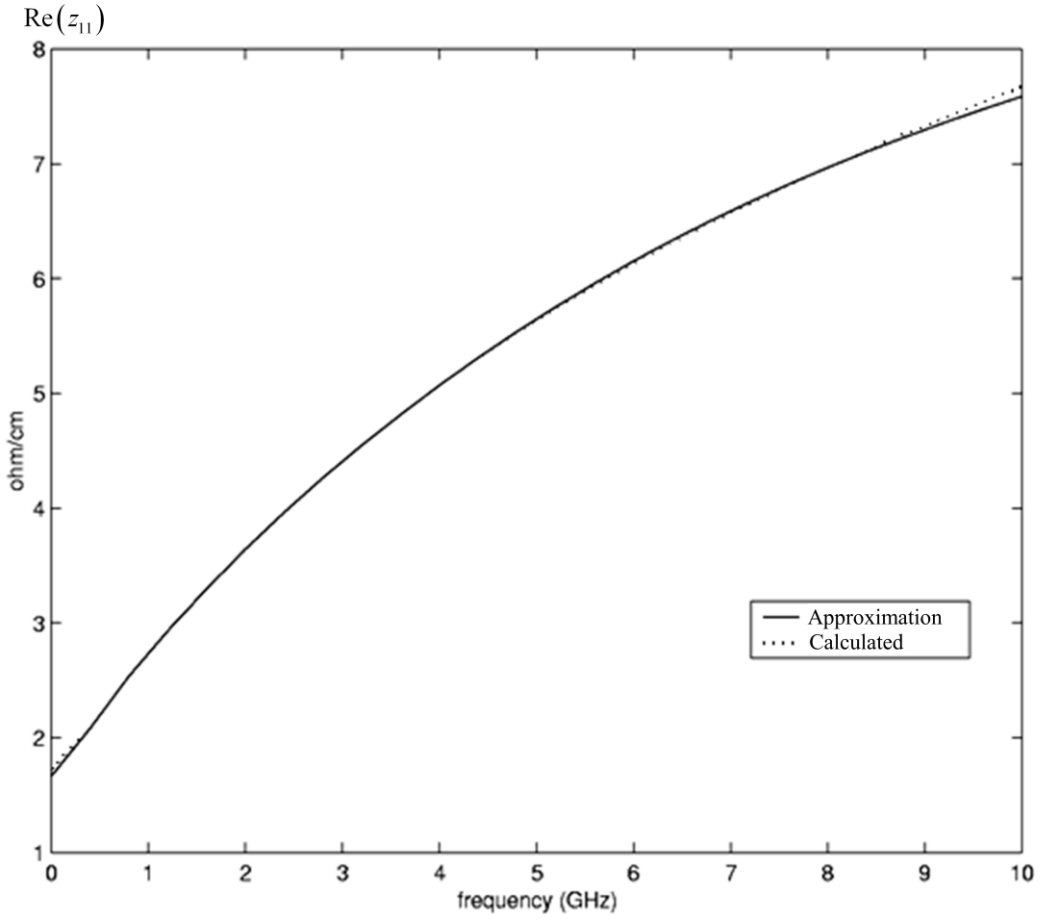

Figure 6.14 Comparison between the Padé approximation of the real part of the p.u.l. impedance z_{11} and the exact value.

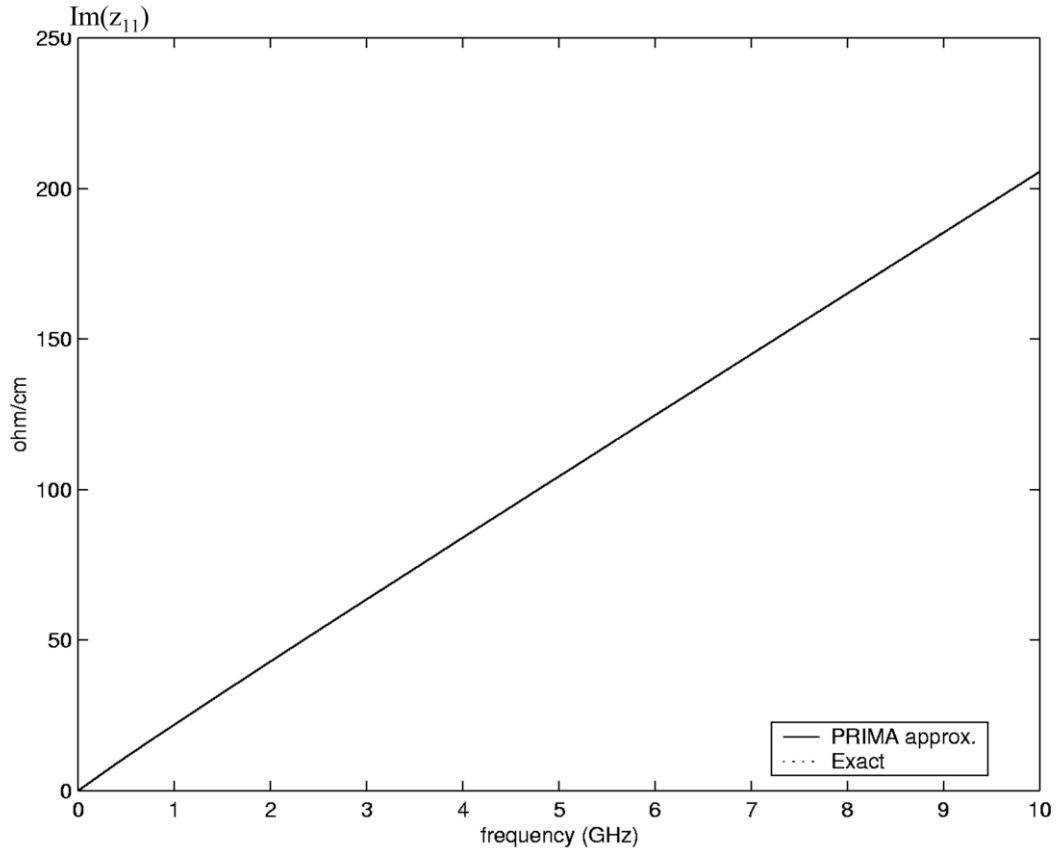

Figure 6.15 Comparison between the Padé approximation of imaginary part of the p.u.l. impedance z_{11} and the exact value.

For the purposes of transient simulation, a trapezoidal pulse of amplitude 5 V, width 3 ns, and rise and fall times of 0.1 ns was used. Figure 6.16 depicts the transient response at the output node 2. In particular, a comparison is provided between the waveforms obtained with and without taking into account the frequency dependence of the p.u.l. resistance and inductance values. The order of the reduced model was 60

and 68 for the frequency independent and frequency dependent models, respectively. The influence of the frequency dependence of the ohmic loss is apparent.

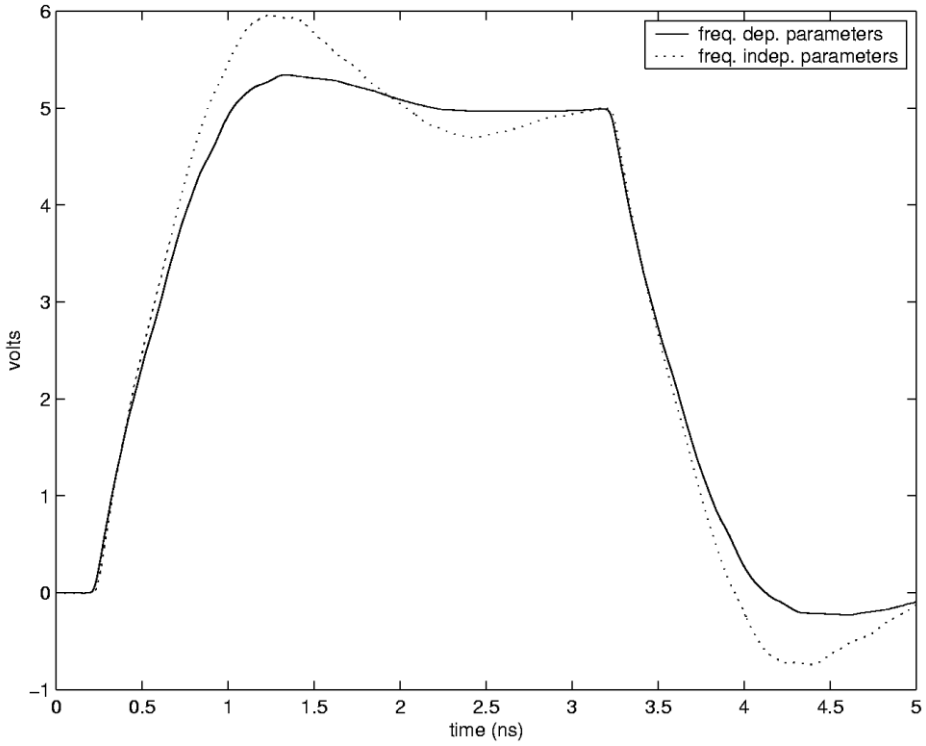

Figure 6.16 Waveform at the output of the active line of the circuit in Figure 6.13.

CHAPTER 7 CONCLUSION

The complexity of high-density circuits is such that the interconnectivity of the devices becomes the impeding factor in achieving desired performance at the system level. Thus, careful modeling of interconnects that accurately captures their behavior over a broad range of frequency is essential. On the other hand, such electrical performance-driven modeling and simulation must be done fast enough to facilitate design iteration and optimization.

An innovative multi-conductor transmission line model has been presented for efficient simulations and passive model order reduction of high speed interconnects. We have proposed three consecutively progressively more complex models that all implement fourth order-accurate compact differences to facilitate highly accurate simulation of multi-GHz bandwidth pulse propagation in multiconductor transmission lines, which use a modest number of about eight degrees of freedom per minimum wavelength of interest. This translates into at least a three-fold reduction in the total number of unknowns required for interconnect simulation when the simple segmentation approach is used. Thus, the proposed models are well suited for efficient simulation of complex interconnection networks containing hundreds of conductors, and in particular wide busses. The discrete models that result from the use of compact differences are passive, and compatible with passive model order reduction techniques such as PRIMA.

In the first model (UA-EPIM), the frequency dependence of ohmic loss is ignored. Such a model is sufficient for less resistive/inductive or slower busses and helps to reduce the number of degrees of freedom. Model order reduction PRIMA can be used for the generation of reduced-order macromodels for complex interconnection networks. Such a small order macromodeling significantly reduces the computational cost of the transient simulation, and thus facilitates sensitivity analysis and driver/load optimization studies.

The second model (UA-DEPIM1), is designed for high-speed dispersive multiconductor interconnection structures with modest coupling. The development of the discrete model is such that the impact of proximity effect on the current distribution over the conductor cross-sections and hence, on the effective value of the p.u.l. resistance and inductance is taken into account. In this model, a scalar order reduction technique has been used to find poles and residues of each diagonal entry of the p.u.l. impedance matrix separately while the frequency dependent off-diagonal elements have been ignored in order to keep the number of unknowns smaller. Once this model is developed, PRIMA can be once again applied to develop a reduced-order, passive macromodel for the interconnection system in a straight forward fashion.

For the third interconnect model (UA-DEPIM2), we have introduced a mathematical model for strongly coupled dispersive multiconductor interconnects which allows for passive model order reduction. The development of the discrete model is such that the impact of proximity effects on the current distribution over the conductor cross-sections, and hence on the effective value of the per-unit-length

resistance and inductance, is taken into account. The proposed methodology employs the modal network theory for the skin effect in lossy conductors and uses PRIMA to generate a passive reduced form of Z(s). Moreover, with proper modification of the governing system of state equations, the reduced form of Z(s) is realizable. Next, with introduction of properly defined auxiliary variables, a discrete model for the Telegrapher's equations is derived which is passive and linear in the Laplace variable *s*. Once this model is developed, PRIMA is applied to develop a reduced-order, passive macromodel for the interconnection system.

A number of single and multi-conductor interconnect circuits were analyzed and each one of proposed methodologies were validated through its application to the transient analysis of the system.

There are a few next steps that come into mind to further improve and extend the development of the proposed discrete models in the future. However, since the time that this work was published in 1999-2000, 168 other publications have so far cited the proposed methodology and some of the improvements to the model have already been implemented. For example, in [21] a rule has been derived for the selection of the order of the reduced model for interconnections modelled as transmission line and its relation to pulse rise time, interconnection length, and physical properties is analysed. In [22], a methodology is presented to obtain poles and residues of the frequency dependent resistance and inductance matrices from a set of values at discrete frequencies that span the frequency bandwidth of interest through a vector-fitting algorithm followed by a passivity check and compensation algorithm. This methodology is specifically helpful when impedance and admittance values for

interconnect transmission lines are available at discrete frequency points through measurements. Another paper [23] proposes a new algorithm to reduce the high-frequency errors beyond $f_{\max}$ in the time-domain macromodels, without increasing the order of the approximation while preserving passivity. The proposed algorithm helps in eliminating spurious ripples in the flat delay portion of transient responses of the distributed network.

Another possible future improvement to the proposed models is to include position dependent impedance and admittance matrices and/or dielectric loss. Such work would enhance the current two dimensional models to three dimensional models and further improve the accuracy of the models.

REFERENCES

[1] A. C. Cangellaris and M. Celik, "Order reduction of high-speed interconnect electrical models: The issue of passivity," *IC/Package Design Integration, 1998. Proceedings. 1998 IEEE Symposium on*. pp. 132–137, 1998.

[2] A. Odabasioglu, M. Celik, and L. T. Pileggi, "PRIMA: passive reduced-order interconnect macromodeling algorithm ," *Computer-Aided Design of Integrated Circuits and Systems, IEEE Transactions on*, vol. 17, no. 8. pp. 645–654, 1998.

[3] P. Silvester, "Modal network theory of skin effect in flat conductors," *Proceedings of the IEEE*, vol. 54, no. 9. pp. 1147–1151, 1966.

[4] C. A. Balanis, *Advanced engineering electromagnetics*. John Wiley & Sons, 1989.

[5] A. C. Cangellaris and R. Lee, "On the accuracy of numerical wave simulations based on finite methods," *J. of Electromagnetic Waves and Applications*, vol. 6, no. 12, pp. 1635–1653, 1992.

[6] O. A. Palusinski and A. Lee, "Analysis of transients in nonuniform and uniform multiconductor transmission lines," *Microwave Theory and Techniques, IEEE Transactions on*, vol. 37, no. 1. pp. 127–138, 1989.

[7] M. Celik, A. C. Cangellaris, and A. Yaghnour, "An all-purpose transmission-line model for interconnect simulation," *Microwave Theory and Techniques, IEEE Transactions on*, vol. 45, no. 10. pp. 1857–1867, 1997.

[8] C. Paul, *Analysis of multiconductor transmission lines*. New York: Wiley, 1992.

[9] S. K. Lele, "Compact finite difference schemes with spectral-like resolution," *Journal of Computational Physics*, vol. 103, no. 1, pp. 16–42, Nov. 1992.

[10] R. W. Newcomb, *Linear Multiport Synthesis*. McGraw-Hill, 1996.

[11] W. T. Weeks, L. L.-H. Wu, M. F. McAllister, and A. Singh, "Resistive and Inductive Skin Effect in Rectangular Conductors," *IBM Journal of Research and Development*, vol. 23, no. 6. pp. 652–660, 1979.

[12] R. W. Freund and P. Feldmann, "Reduced-order modeling of large passive linear circuits by means of the SyPVL algorithm," *Computer-Aided Design,*

1996. ICCAD-96. Digest of Technical Papers., 1996 IEEE/ACM International Conference on. pp. 280–287, 1996.

[13] L. T. Pillage and R. A. Rohrer, "Asymptotic waveform evaluation for timing analysis," *Computer-Aided Design of Integrated Circuits and Systems, IEEE Transactions on*, vol. 9, no. 4. pp. 352–366, 1990.

[14] M. K. L. Miguel Silveira Jacob White, "Efficient Reduced-Order Modeling of Frequency-Dependent Coupling Inductances associated with 3-D Interconnect Structures," *Design Automation, 1995. DAC '95. 32nd Conference on*. pp. 376–380, 1995.

[15] D. F. Anastasakis, N. Gopal, S.-Y. Kim, and L. T. Pillage, "Enhancing the stability of asymptotic waveform evaluation for digital interconnect circuit applications," *Computer-Aided Design of Integrated Circuits and Systems, IEEE Transactions on*, vol. 13, no. 6. pp. 729–736, 1994.

[16] E. Chiprout and M. S. Nakhla, "Analysis of interconnect networks using complex frequency hopping (CFH)," *Computer-Aided Design of Integrated Circuits and Systems, IEEE Transactions on*, vol. 14, no. 2. pp. 186–200, 1995.

[17] M. Celik, O. Ocali, M. A. Tan, and A. Atalar, "Pole-zero computation in microwave circuits using multipoint Pade approximation," *Circuits and Systems I: Fundamental Theory and Applications, IEEE Transactions on*, vol. 42, no. 1. pp. 6–13, 1995.

[18] L. Miguel Silveira, M. Kamon, I. Elfadel, and J. White, "A coordinate-transformed Arnoldi algorithm for generating guaranteed stable reduced-order models of RLC circuits," *Computer-Aided Design, 1996. ICCAD-96. Digest of Technical Papers., 1996 IEEE/ACM International Conference on*. pp. 288–294, 1996.

[19] K. J. Kerns, I. L. Wemple, and A. T. Yang, "Stable and efficient reduction of substrate model networks using congruence transforms," *Computer-Aided Design, 1995. ICCAD-95. Digest of Technical Papers., 1995 IEEE/ACM International Conference on*. pp. 207–214, 1995.

[20] M. Celik and A. C. Cangellaris, "Simulation of multiconductor transmission lines using Krylov subspace order-reduction techniques," *Computer-Aided Design of Integrated Circuits and Systems, IEEE Transactions on*, vol. 16, no. 5. pp. 485–496, 1997.

[21] A. C. Cangellaris and M. Igarashi, "Rules for robust generation of accurate reduced-order models of high-speed coupled interconnections," *Electronic Components & Technology Conference, 2000. 2000 Proceedings. 50th*. pp. 502–507, 2000.

[22] M. Tang and J. Mao, "A compact passive model of transmission lines with frequency-dependent parameters," *Microwave and Millimeter Wave*

Technology (ICMMT), 2010 International Conference on. pp. 1555–1558, 2010.

[23] A. Dounavis, R. Achar, and M. S. Nakhla, "Addressing transient errors in passive macromodels of distributed transmission-line networks," *Microwave Theory and Techniques, IEEE Transactions on*, vol. 50, no. 12. pp. 2759–2768, 2002.

[24] R. Rohrer and H. Nosrati, "Passivity considerations in stability studies of numerical integration algorithms," *Circuits and Systems, IEEE Transactions on*, vol. 28, no. 9. pp. 857–866, 1981.

[25] D. Saraswat, R. Achar, and M. S. Nakhla, "Passive reduction algorithm for RLC interconnect circuits with embedded state-space systems (PRESS)," *Microwave Theory and Techniques, IEEE Transactions on*, vol. 52, no. 9. pp. 2215–2226, 2004.

[26] I. M. Elfadel, A. Dounavis, H.-M. Huang, M. S. Nakhla, A. E. Ruehli, and R. Achar, "Accuracy and performance of passive transmission line macromodels based on optimal matrix rational approximations," *Electrical Performance of Electronic Packaging, 2002*. pp. 351–354, 2002.

[27] M. T. Bohr, "Interconnect scaling-the real limiter to high performance ULSI," *Electron Devices Meeting, 1995., International*. pp. 241–244, 1995.

[28] E. E. Davidson, B. D. McCredie, and W. V. Vilkelis, "Long lossy lines (L^3) and their impact upon large chip performance," *Components, Packaging, and Manufacturing Technology, Part B: Advanced Packaging, IEEE Transactions on*, vol. 20, no. 4. pp. 361–375, 1997.

[29] L. Schaper, M. Dibbs, P. Garrou, C. C. Chau, Y. So, D. Frye, J. Wagner, J. Ousley, G. Baugher, R. Picard, G. Connor, D. Winn, P. Deane, R. Eden, and R. Sands, "Seamless high off-chip connectivity [IC packaging]," *IC/Package Design Integration, 1998. Proceedings. 1998 IEEE Symposium on*. pp. 39–44, 1998.

[30] R. R. Tummala and E. J. Rumaszewski, *Microelectronics Packaging Handbook*, 2nd ed. New York: Chapman & Hall, 1997.

[31] A. Semlyen and A. Dabuleanu, "Fast and accurate switching transient calculations on transmission lines with ground return using recursive convolutions," *Power Apparatus and Systems, IEEE Transactions on*, vol. 94, no. 2. pp. 561–571, 1975.

[32] T. K. Tang and M. S. Nakhla, "Analysis of high-speed VLSI interconnects using the asymptotic waveform evaluation technique," *Computer-Aided Design of Integrated Circuits and Systems, IEEE Transactions on*, vol. 11, no. 3. pp. 341–352, 1992.

[33] S.-Y. Kim, N. Gopal, and L. T. Pillage, “Time-domain macromodels for VLSI interconnect analysis,” *Computer-Aided Design of Integrated Circuits and Systems, IEEE Transactions on*, vol. 13, no. 10. pp. 1257–1270, 1994.

[34] E. Chiprout and M. S. Nakhla, *Asymptotic Waveform Evaluation and Moment Matching for Interconnect Analysis*. Kluwer Academic Publishers, 1994.

[35] P. Feldmann and R. W. Freund, “Efficient linear circuit analysis by Pade approximation via the Lanczos process,” *Computer-Aided Design of Integrated Circuits and Systems, IEEE Transactions on*, vol. 14, no. 5. pp. 639–649, 1995.

[36] K. Gallivan, E. Grimme, and P. Van Dooren, “Asymptotic waveform evaluation via a Lanczos method,” *Applied Mathematics Letters*, vol. 7, no. 5, pp. 75–80, Sep. 1994.

[37] M. Celik and A. C. Cangellaris, “Simulation of dispersive multiconductor transmission lines by Pade approximation via the Lanczos process,” *Microwave Theory and Techniques, IEEE Transactions on*, vol. 44, no. 12. pp. 2525–2535, 1996.

[38] C. Paul, *Analysis of Multiconductor Lines*. New York: Wiley Interscience, 1992.

[39] M. Celik and A. C. Cangellaris, “A general dispersive multiconductor transmission line model for interconnect simulation in SPICE,” *Computer-Aided Design, 1996. ICCAD-96. Digest of Technical Papers., 1996 IEEE/ACM International Conference on*. pp. 563–568, 1996.

[40] A. C. Cangellaris, M. Celik, S. Pasha, and L. Zhao, “Electromagnetic model order reduction for system-level modeling,” *Microwave Theory and Techniques, IEEE Transactions on*, vol. 47, no. 6. pp. 840–850, 1999.

[41] A. C. Cangellaris, S. Pasha, J. L. Prince, and M. Celik, “A new discrete transmission line model for passive model order reduction and macromodeling of high-speed interconnections,” *Advanced Packaging, IEEE Transactions on*, vol. 22, no. 3. pp. 356–364, 1999.

[42] S. Pasha, A. C. Cangellaris, and J. L. Prince, “An all purpose dispersive multiconductor interconnect model compatible with PRIMA,” *Electronic Components & Technology Conference, 2000. 2000 Proceedings. 50th*. pp. 513–517, 2000.

[43] S. Pasha, A. C. Cangellaris, and J. L. Prince, “An all-purpose dispersive multiconductor interconnect model compatible with PRIMA,” *Advanced Packaging, IEEE Transactions on*, vol. 24, no. 2. pp. 126–131, 2001.

[44] S. Pasha, A. C. Cangellaris, J. L. Prince, and M. Celik, “Passive model order reduction of multiconductor interconnects,” *Electrical Performance of Electronic Packaging, 1998. IEEE 7th Topical Meeting on*. pp. 291–294, 1998.

[45] S. Pasha, M. Celik, A. C. Cangellaris, and J. L. Prince, “Passive SPICE-compatible models of dispersive interconnects,” *Electronic Components and Technology Conference, 1999. 1999 Proceedings. 49th*. pp. 493–499, 1999.